Temperature dependent magnetic properties of ZrO_2 coated $CoFe_2O_4$ nanoparticles
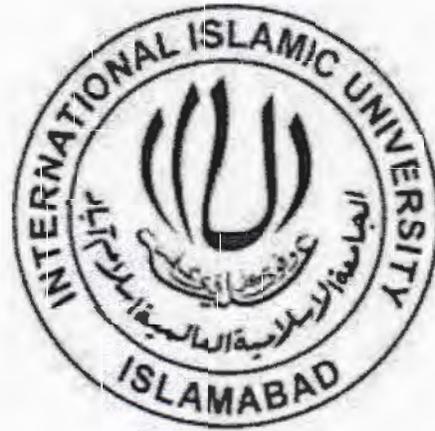
by:

Syed Zaeem-ul-Hassan

(350-FBAS/MSPHY/F15)

Supervisor:

Dr. Kashif Nadeem

Assistant Professor
Department of Physics, FBAS, IIUI

**Department of Physics Faculty of Basic and Applied Sciences
International Islamic University, Islamabad**

(2017)

i

Nanotechnology

Nanoparticles

Magnetism

Ferrites

Cobalt ferrite

Zirconia

X-Ray- diffraction

Temperature dependent magnetic Properties of ZrO_2 coated $CoFe_2O_4$ nanoparticles

by:

Syed Zaeem-ul-Hassan
(350-FBAS/MSPHY/F15)

This thesis is submitted to Department of Physics International Islamic University, Islamabad for the award of degree of MS Physics

Chairman, Department of Physics
International Islamic University, Islamabad

Dean Faculty of Basic and Applied Science
International Islamic University, Islamabad

**Department of Physics Faculty of Basic and Applied Sciences
International Islamic University, Islamabad**

ii

Final Approval

It is certified that the work printed in this thesis entitled **"Temperature dependent magnetic properties of ZrO$_2$ coated CoFc$_2$O$_4$ nanoparticles** by **Syed Zaeem-ul-Hassan** (registration No.350-FBAS/ MSPHY/F15) is of sufficient standard in scope and quality for award of degree of MS Physics from Department of Physics, International Islamic University, Islamabad, Pakistan.
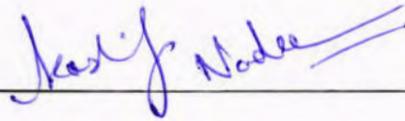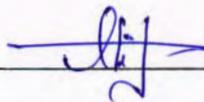
Viva Voce Committee

Chairman _____
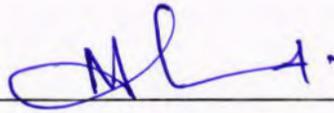
(Department of Physics)

Supervisor _____

External Examiner _____

Internal Examiner _____

بسم الله الرحمن الرحيم

DEDICATED

To

My

Beloved Parents

And

Respected Teachers

Declaration

I, Syed Zaeem-ul-Hassan (Registration # 350-FBAS/MSPHY/F15), student of MS in Physics (session 2015-2017), hereby declare that the work presented in the thesis entitled "Temperature dependent magnetic properties of ZrO_2 coated $CoFe_2O_4$ nanoparticles" is my own work and has not been published or submitted as research work or thesis in any form in any other university or institute in Pakistan or aboard.
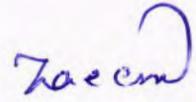
Syed Zaeem-ul-Hassan

(350-FBAS/MSPHY/F15)

Dated: 29-08-2017

FORWARDING SHEET BY RESEARCH SUPERVISOR

The thesis entitled **"Temperature dependent magnetic properties of ZrO$_2$ coated CoFe$_2$O$_4$ nanoparticles"** submitted by **Syed Zaeem-ul-Hassan** in partial fulfillment of M.S. degree in Physics has been completed under my guidance and supervision. I am satisfied with the quality of his research work and allow him to submit this thesis for further process to graduate with Master of Science degree from Department of Physics, as per IIU rules and regulations.

Dated: __29-08-2017__
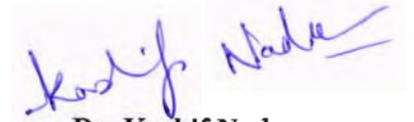
Dr. Kashif Nadeem,
Assistant Professor
Department of Physics,
International Islamic University,
Islamabad.

ACKNOWLEDGMENT

Table of Contents

List of Figures

List of Table

ABSTRACT

We have studied temperature dependent magnetic properties of ZrO_2 coated cobalt ferrite ($CoFe_2O_4$) nanoparticles prepared by microwave plasma synthesis. Crystal structure of nanoparticles was determined by using X-ray diffraction which confirms the inverse spinel structure of $CoFe_2O_4$ nanoparticles. The average crystallite size of nanoparticles was calculated by Debye Scherer's formula and found 13 nm. Morphology of nanoparticles was observed by transmission electron microscopy (TEM). TEM image showed that the nanoparticles are spherical in shape and less agglomerated. The average blocking temperature (T_B) was above 300 K as evident by ZFC curve. The saturation magnetization (M_s) value was 20 emu/g at 5 K which is much lower than bulk value of $CoFe_2O_4$ (80 emu/g) due to finite size and surface effects. The M_s showed an increasing trend with decreasing temperature from 300 to 5 K due to decrease in thermal fluctuations of magnetic moments. Bloch's law was fitted to T-dependent M_s data and it showed lower value of Bloch's exponent as compared to bulk $CoFe_2O_4$. The value of coercivity increases with decreasing temperature and sharp increase was observed below 50 K due to contribution of large surface anisotropy. Kneller's law showed a good fit for T-depended coercivity (H_c) data. Stretched exponential law ensured slow spin dynamics in ZFC protocol due to presence of spin glass behavior at 5 K. In summary, non-magnetic ZrO_2 coated $CoFe_2O_4$ nanoparticles showed enhanced surface anisotropy and possible weak spin glass behavior at low temperature due to pinned surface spins.

CHAPTER 1

Introduction

1.1   Nanoscience

Nanoscience is a study of materials at nano-scale ranging from 1 to 100 nm. Nanoscience is the combination of two words, which is derived from Greek language. Nano means "Dwarf" (extremely small size up to 10^{-9}) and science means scientific knowledge [1]. One nanometer refers to a billionth of a meter.

1.2   Nanotechnology

Nanotechnology deals to the branch of a technology, in which we study the materials with size in the range of 1 to 100 nm. Especially the manipulation of a matter and its structural assembling with atoms or molecules is important at nm scale [2].
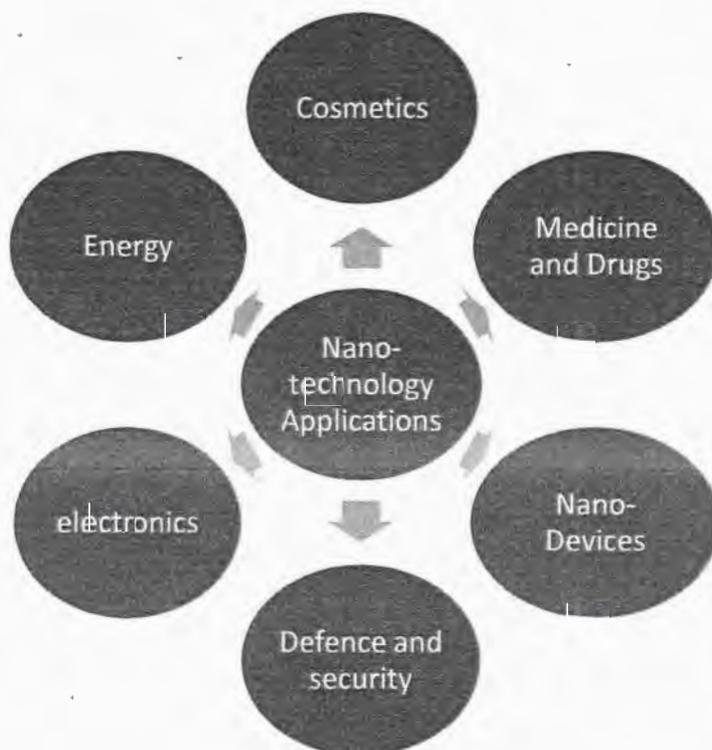
Fig. 1.1: Applications of nanotechnology.

Nanotechnology contributes in all major sciences including physics, biology, molecular engineering and chemistry etc. Nanotechnology possess unique physical,

chemical, optical and mechanical properties after the manipulation of matter at nano-scale [3]. Nanotechnology possess diverse promising applications in various fields like cosmetics, energy, engineering, medicine, defense, semiconductor industry, security and electronics [4] as shown in Fig. 1.1.

1.2.1 History of Nanotechnology

A word of Nanotechnology was originated from the Greek language in which 'Nano' means "particularly very small" and technology means "scientific knowledge" [5]. The first basic concept of nanotechnology was discussed since 1959 by famous professor, Richard Feynman. He presented this 'There is a plenty of the room at Bottom" [6].

1.3 Nanoparticles

Nanoparticles are particles with diameter in the range from 1 to 100 nm. Nanoparticles are formed by a collection of atoms bounded together and its radius should be less than 100 nm [7]. At nano-scale, the magnetic, mechanical and electric properties of the nanoparticles are entirely diverse as compared to bulk particles due to large surface to the volume ratio and high surface energy. Nanoparticles can be developed by two process of approaches such as top-down and bottom-up [8].

1.3.1 Top down approach

The development of nanoparticles in the case of top-down approach initially begins with bulk material and converts it into the smaller particles. Milling is an example of top down approach for preparing nanoparticles. There is a huge difficulty in the top down approach which occur due to deficiency in particles structure [9]. Such a deficiency can contribute in physical properties and, alter the chemistry of surface in nano-structure and nano-materials. Top down synthesis approach raise internal stress and accumulation in defects on the surface as well as contamination.

1.3.2 Bottom up approach

If the solid material is developed by combining atom with atom, molecule by molecule and cluster through cluster then solid material is constructed through bottom up

approach. Solid materials constructed through bottom up approach possess less defects, high purity and gives controlled particle size [10]. The schematic diagram of bottom up approach and top down approach is shown in Fig. 1.2.

(a) Bottom-up approaches   (b) Top-down approaches
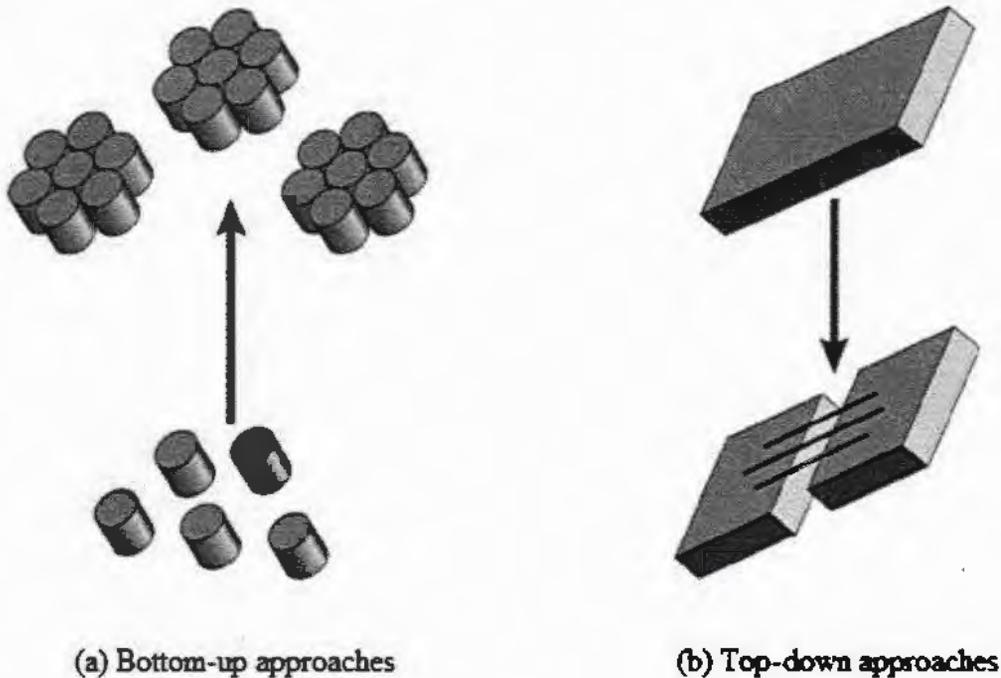
Fig. 1.2: (a) Bottom-up approach (b) Top-down approach [11].

1.4   Magnetism

The phenomena of magnetism associated with the magnetic field that arises from the flow of electric charge. There are two types of motions of electron which can generate magnetic field. One is a spin motion might be up and down and other one is orbital motion in which electrons revolve around a nucleus [12]. The magnetic field could be detected by entering or existing in the material is known as magnetic dipole. Magnetic pole could not be identified in an isolation state, it always dipole state. Consider a bar magnetic which possesses two poles, one end is north and another end is South pole. In this equation div.B = 0, Maxwell mentioned that mono-pole does not exist.

Magnetization 'M' is defined as the magnetic moment per unit volume as given below in equation (1.1),

$$M = \mu / V \qquad (1.1)$$

In addition, the magnetization is a function of magnetic susceptibility (χ_m) along with magnetic field intensity (H).

$$M = \chi_m H \qquad (1.2)$$

In free space, magnetization is the zero relation of magnetic field as given in below equation,

$$B = \mu_0 H \qquad (1.3)$$

where 'μ_0' is equal to $4\pi \times 10^{-7}$ H-m^{-1}

In the case of solid material, where M is not equal to zero in equation given below,

$$B = \mu_0 (M+H) \qquad (1.4)$$

For the linear magnetization of magnetic materials, we have

$$M = \chi H \qquad (1.5)$$

Using equations (1.4) and (1.5), we have

$$B = \mu_0 (H + \chi H) \qquad (1.6)$$

Finally,

$$B = \mu_0 (1+\chi) H \qquad (1.7)$$

Where $\mu_r = (1+\chi)$ is the value of relative permeability, from equation (1.7)

$$B = \mu_0 \mu_r H \qquad (1.8)$$

Equation (1.8) exhibits the linear relation of magnetic induction and magnetic field strength.

1.4.1 Origin of magnetism

Magnetic moment plays a vital role in the field of magnetism. It is defined as the vector product of current 'I' is generated due to electrons revolve around a nucleus and area 'A' of the circular loop as represented in Fig.1.3.

$$M = I.A \hspace{5cm} (1.9)$$
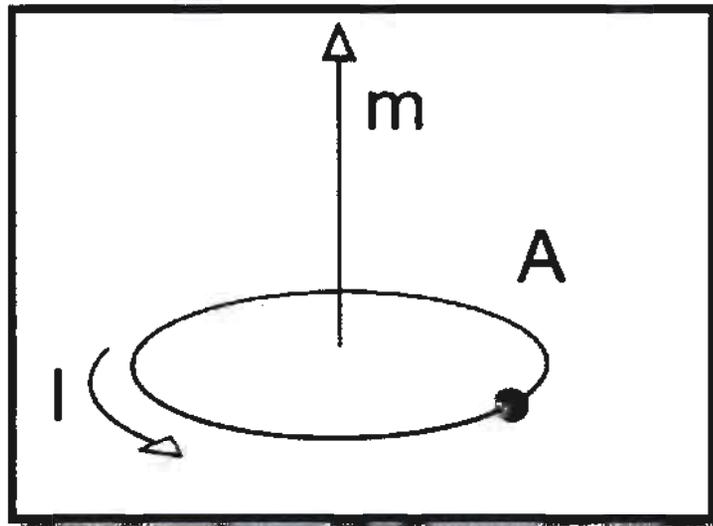
Fig. 1.3: Phenomena of dipole moment [13].

In Fig. 1.3, two arrows indicate the direction of magnetic moment and the current that revolves in the form of electron orbital motion. Magnetic moment is a vector quantity. It has standard unit A/m^2. There are two sources of magnetic moment involve in magnetism. Magnetic moment can be generated by the orbital motion of charge particles and the magnetic moment generated due to spinning of electrons around its own axis as shown in Fig. 1.4.
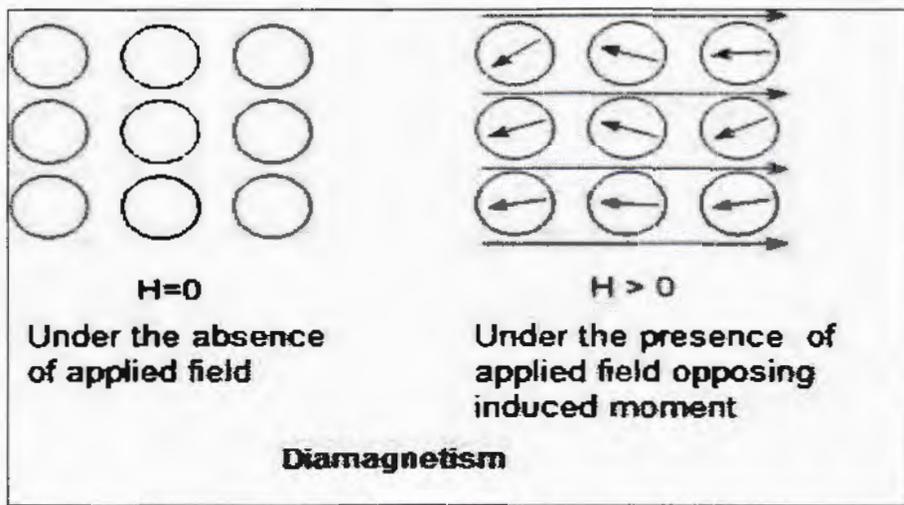
Fig. 1.5: Phenomena of diamagnetism in absence and presence of H [16].

When diamagnetic material is placed in the external magnetic field, magnetization occurs in opposite direction to the applied field. It means these materials oppose to applied field [17]. In diamagnetism, the atoms do not possess permanent dipole magnetic moments. Diamagnetic effect can be observed in those materials in which atoms have paired electrons in the orbital shells [18].
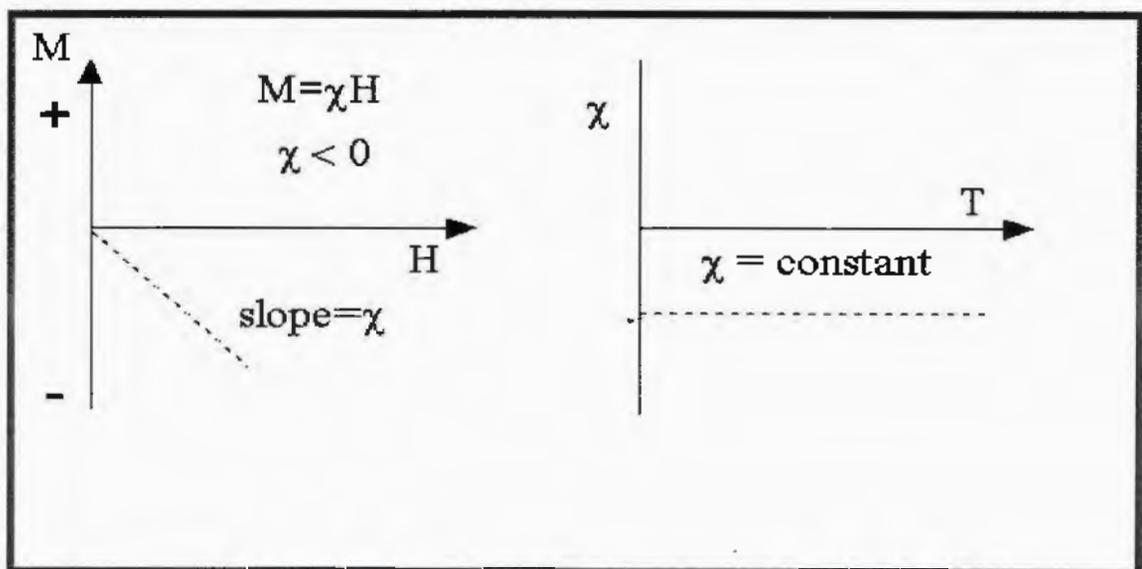
Fig. 1.6: Diamagnetism curve for M vs. H and χ vs. T [19].

The magnetic susceptibility of the diamagnetic materials is independent of temperature. When external field is applied to diamagnetic materials, magnetic moments aligned themselves opposite to the applied field which results negative susceptibility in diamagnetic materials as shown in Fig. 1.6. There are various examples of diamagnetic materials like copper, bismuth, Gold, Mercury, Tin and zinc etc.

1.5.2 Paramagnetism

Materials which exhibit phenomena of paramagnetism possess unpaired electrons. These electrons aligned in a particular order in the atomic shells. This is the property of the paramagnetic materials that magnetic moments align themselves in a random fashion when there is no applied magnetic field. When we apply the external magnetic field, all the magnetic moments follow the direction of applied magnetic field [20]. In the absence of applied magnetic field, random magnetic moments in paramagnetic materials result zero magnetization. While in case of external magnetic field, magnetic moments align themselves and give nonzero magnetization in the system. The sketch of magnetic moments of paramagnetic materials in absence of applied field and in case of applied field is shown in Fig.1.7.
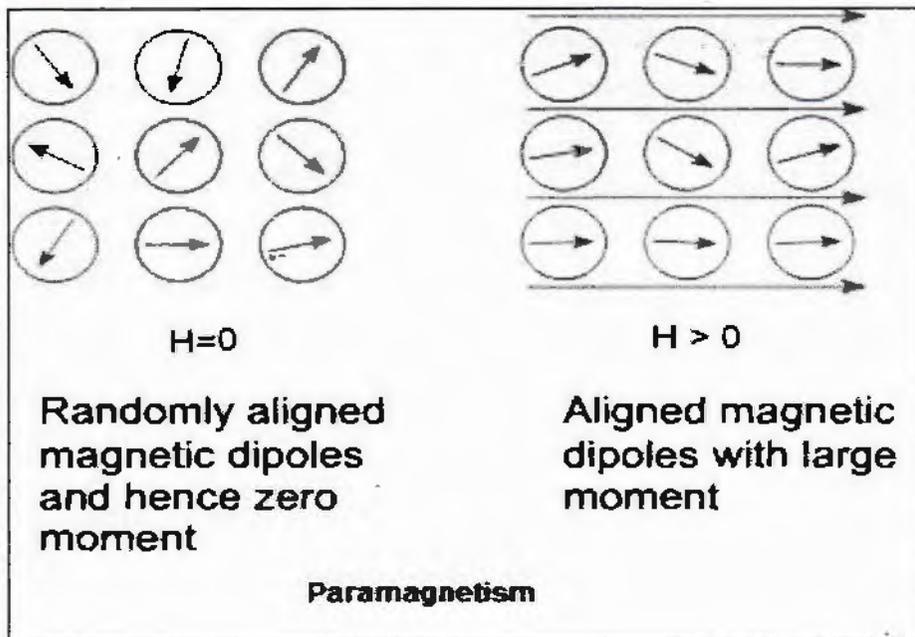
Fig. 1.7. Phenomena of paramagnetism [16].

Paramagnetic materials show small magnetic susceptibility and the main reason behind this is the randomness of the magnetic moments in the absence of the applied magnetic field, which get aligned in the presence of applied magnetic field. Paramagnetic materials possess ability to attract magnet. There are various examples of paramagnetic materials such as manganese, potassium, palladium and tungsten etc. [21]. Temperature strongly effects on the magnetism of paramagnetic materials. If the temperature gradually increases, it affects the randomly oriented dipole moments which results increased in material's thermal agitation. Under the application of small magnetic field on paramagnetic materials results nonzero net magnetization and by increasing "H" the induced magnetization increases linearly as shown in Fig. 1.8.
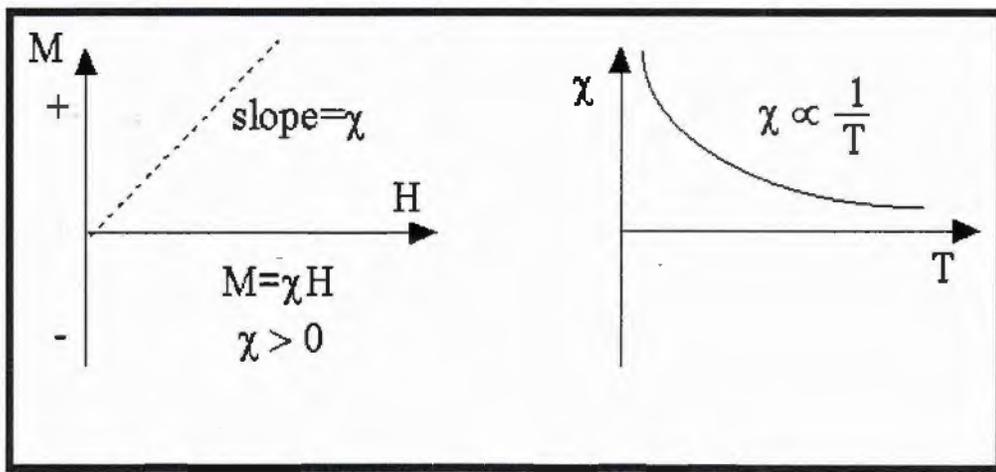
Fig. 1.8: M vs. H plot and χ vs. T curve for paramagnetic materials [16].

1.5.3 Ferromagnetism

Materials which exhibit the phenomena of ferromagnetism possess permanent magnetic moment under the absence of applied external magnetic field [22]. It is due to the presence of spontaneous magnetization. In ferromagnetic materials, all magnetic moments are aligned. Ferromagnetic materials have spontaneous magnetization [23]. Ferromagnetic bulk materials consist of multi-domains and separated by domain walls as shown in Fig. 1.9. Each domain possesses magnetic moment in one direction and all domains in the material are randomly oriented with respect to each other. Each domain has volume 10^{-8} - 10^{-12} m^3 and the thickness of domain wall is about 100 nm. When ferromagnetic material is placed in external magnetic field, all domains tend to rotate

themselves in the direction of applied field. As the applied magnetic field value increased, magnetization also increases. Ferromagnetic materials have ability to attract magnet. Examples of ferromagnetic materials include nickel, iron and cobalt.
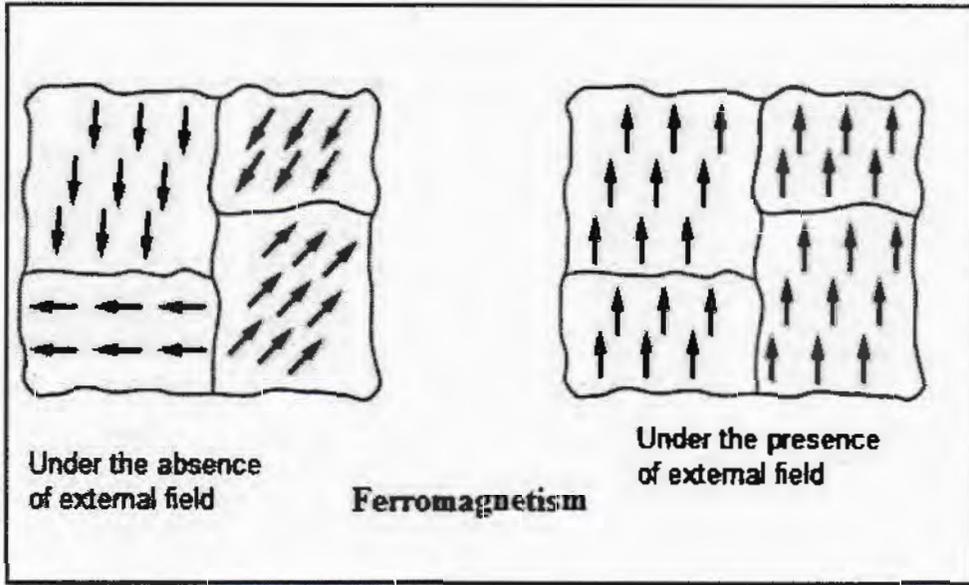
Fig. 1.9: Schematic diagram of ferromagnetism in absence and presence of H [24].

1.5.4 Anti-ferromagnetism

Antiferromagnetic materials belong to a class of magnetic materials in which magnetic spins have equal magnitude and align themselves opposite to each other as shown in Fig. 1.10. In the antiferromagnetic materials, antiparallel alignment of the magnetic moments results no net magnetization in the absence of the applied external magnetic field [25].
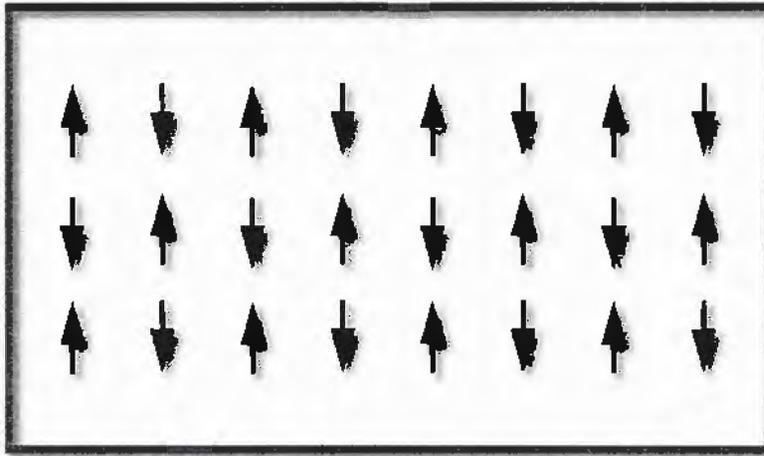
Fig. 1.10: Anti-ferromagnetic material possess spins with equal magnitude but opposite direction [26].

When antiferromagnetic materials are placed in external magnetic field, small magnetization induces along the direction of external field which is gradually increased with increasing temperature till transition stage as shown in Fig 1.11. The transition temperature of antiferromagnetic materials is known as Neel temperature. Above the Neel temperature antiferromagnetic behavior change to paramagnetic one and magnetic susceptibility of antiferromagnetic material is given below,

$$\chi = C / (T+T_N) \qquad\qquad (1.10)$$

Where 'C' is curie constant and mainly it depends upon material's properties. There are various examples of anti-ferromagnetic material such as nickel oxide (NiO) and manganese oxide (MnO) etc.
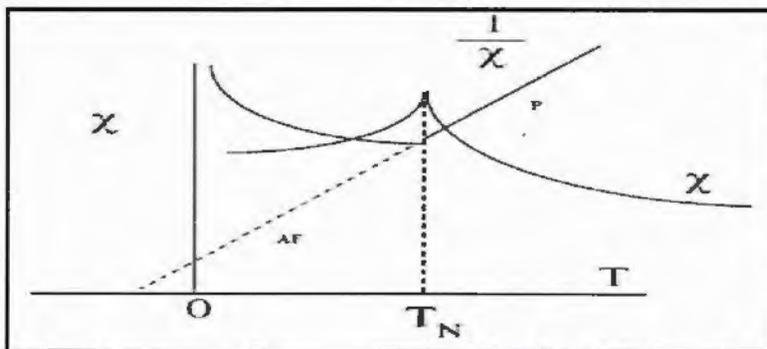
Fig. 1.11: Temperature dependence of the magnetic susceptibility for anti-ferromagnetic materials [19].

1.5.5 Ferrimagnetism

Ferrimagnetism is quite like anti-ferromagnetism but difference lies in the magnitude of the magnetic moments which is not equal in the case of ferrimagnetism. Both materials possess spontaneous magnetization. Ferrites are composed of ferrimagnetic materials and behave as permanent magnet after the application of applied external magnetic field [27]. Ferrimagnetic materials belong to a class of magnetic materials in which magnetic moments on the sub lattice are not equal and these magnetic moments are anti-parallel in direction. In the ferrimagnetic materials magnetic moments cancel out each other effect up to some extent but net magnetization is still there as shown in Fig. 1.12.
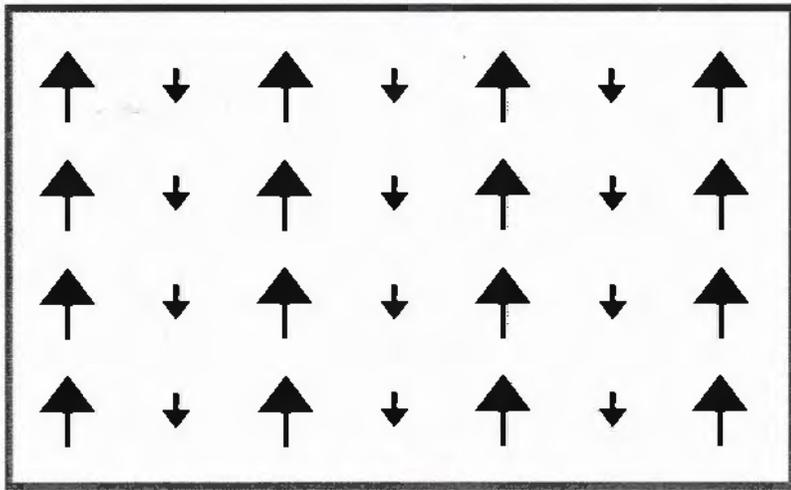
Fig. 1.12: Ferrimagnetism having unequal magnitude and opposite spins [28].

Ferrimagnetic state of the material is temperature dependent and after this state, these materials convert to paramagnetic one. Ferrimagnetic materials are those one which possess positive and high susceptibility as compared with other material such as diamagnetic and paramagnetic. Moreover ferrimagnetic material possesses spontaneous magnetization below Neel temperature because magnetic spins are magnetically ordered, while above T_N dipole moments are completely misaligned and material becomes

paramagnetic. There are various examples of ferrimagnetic materials such as nickel ferrite and magnetite.

1.6   Superparamagnetism

Superparamagnetic materials consist of single domain particles and freely rotate about their easy axis under the absence of external magnetic field. When we apply the external applied magnetic field, magnetic moments follow the direction of applied magnetic field. In the absence of external field magnetization goes to zero and behave as nonmagnetic material [29]. Superparamagnetic materials do not possess hysteresis loop as shown in Fig. 1.13.
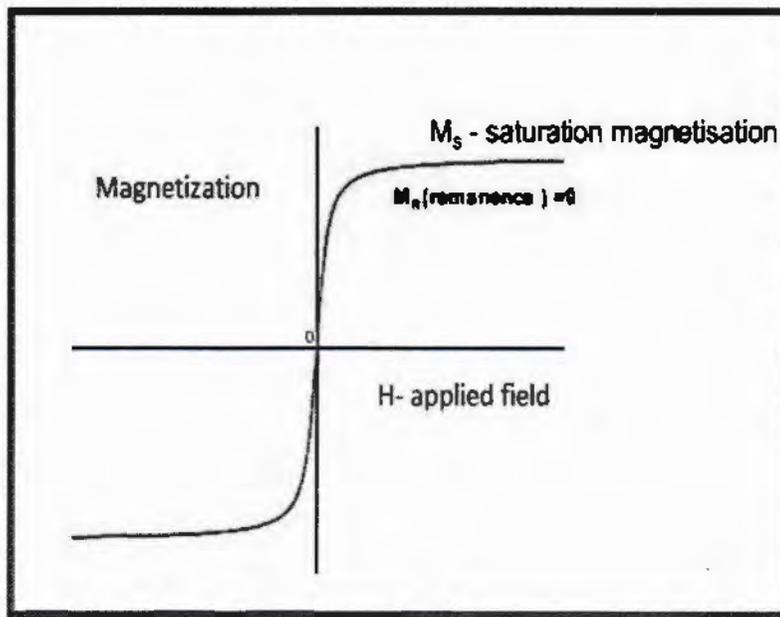
Fig. 1.13: M-H curve for superparamagnetic materials [30].

While moving from multi-domain to single-domain as we decrease the particle size and the coercivity value increases. When we approach the size of single domain particle, the coercivity starts to decrease and it becomes zero in superparamagnetic region. Fig. 1.14 shows the trend of coercivity with size of the particle.
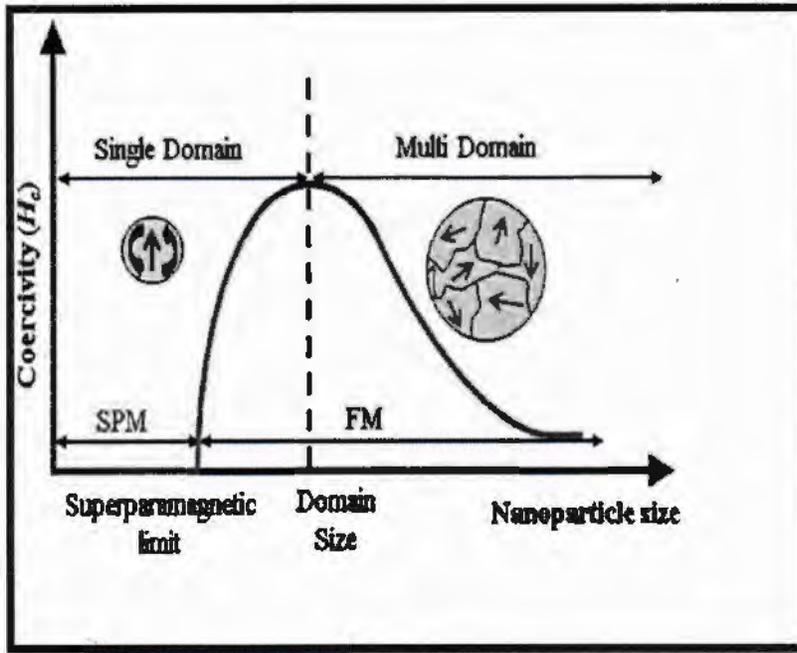
Fig. 1.14: Relation between coercivity vs. particles size [31].

Superparamagnetic behavior is observable for the particles having size in the range of 1-10 nm and possess short relaxation time than experimental time [32]. Moreover, the transition from superparamagnetic to freezing state at blocking temperature is expressible by an equation known as Neel-brown relaxation model.

$$\tau_m = \tau_o \exp(KV/k_BT_B) \tag{1.11}$$

In equation 1.11, where "K" is the anisotropy constant, "V" is the volume of particle and k_BT_B is thermal energy. Whenever measurement time is less than the spin flip time ($\tau_m < \tau_o$), it means particle is in blocked state. However, if measurement time is higher than the spin flip time ($\tau_m > \tau_o$), than the particle will be in superparamagnetic state and this spin-flip mechanism is represented in Fig.1.15.

14

$$\Delta E = K_u V$$
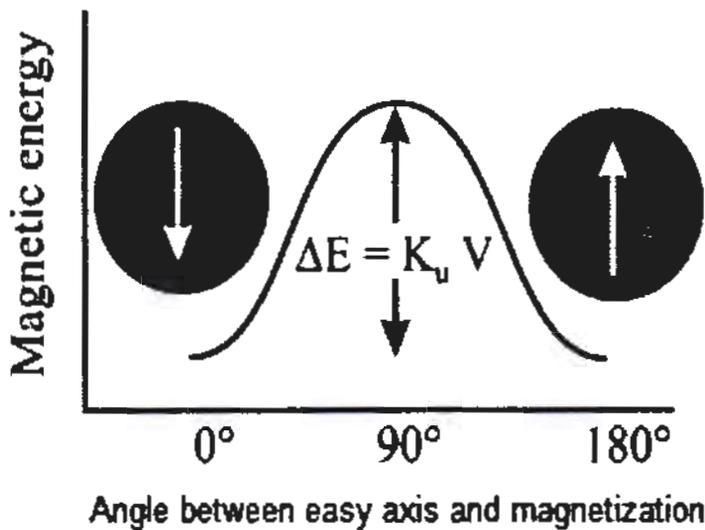
Fig. 1.15: Spin-flip mechanism [33].

1.7   Ferrites

Ferrites belong to class of ceramic materials which are composed of iron oxide and metallic components. Ferrites are basically ferrimagnetic materials and possess electrically insulating behavior [34]. The chemical formula of ferrites is AB_2O_4, where "A" stands for divalent metal ion like Mg and "B" refers to trivalent ion such as Fe. Ferrites have diverse and remarkable properties such as high Curie temperature, great chemical stability, low eddy current loses and low dielectric losses. Ferrites are further divided into two groups. 1st is soft ferrites and 2nd one is hard ferrites.

1.7.1 Soft ferrites

Soft ferrites are those materials which can be easily magnetized or demagnetized. Soft ferrites have low remanence and coercivity [35]. Moreover, soft ferrites contain spinel structure with general chemical formula is XFe_2O_4, where X stands for divalent ions like Co, Fe and Mg. Soft ferrites have many significant properties including higher saturation magnetization and low eddy loss of current etc. Soft ferrites material possess very thin hysteresis loop which is mainly due to possessing low coercivity. Soft ferrites are iron, manganese and cobalt material that are used in many extensive applications like transformer, line filter, and excellent power conversion [36].

1.7.2 Hard ferrites

Hard ferrites hardly magnetized and demagnetized. Due to high remanence, these materials are more appropriate for permanent magnets [37]. Hysteresis loops of hard ferrites possess larger area as compared to hysteresis loops of soft ferrites due to high coercivity and high remanence. Hard ferrites are used in refrigerators, air craft's and loud speakers because of their versatile properties [38].

1.8   Spinel ferrites

Spinel ferrites are also known as cubic ferrites. They are divided into different categories like normal spinel, inverse spinel and mixed spinel. Spinel ferrites are employed innumerous applications such as in magnetic tools, microwave frequencies because of low eddy current losses and high electrical resistivity. Unit cell of spinel ferrites contains fifty-six ions. In which, 32 are oxygen anions, 8 divalent cation ions and 16 trivalent cations. There are two different sites over which metallic cation be placed and these sites are referred as A and B or tetrahedral and octahedral respectively. A site, which can occupy 64 ions and B can 32 ions for each unit cell of spinel ferrite. General chemical formula of spinel ferrite is MN_2O_4 , where M is represented to divalent metal ion and B site referred to trivalent ions [39].

1.9   Types of spinel ferrites

Spinel ferrites are classified into following categories as mentioned below,

1-   Normal spinel

2-   Inverse spinel

3-   Mixed spinel

1.9.1 Normal spinel ferrites

The normal spinel ferrites possess general formula $(G^{+2})[H^{+3}_2]O_4$ where G represents to (A) sites and H refers to (B) sites. The divalent cations G^{+2} are situated at

16

tetrahedral sites, while trivalent cations H^{+3} occupy the octahedral sites [40]. There are many examples of normal spinel ferrites such as zinc ferrite ($ZnFe_2O_4$).

1.9.2 Inverse spinel ferrites

Inverse Spinel ferrites possess general formula $[H^{+3}][G^{+2}H^{+3}]O_4$ where half of trivalent ions (H^{3+}) prefer to go over tetrahedral site and half on octahedral site. While divalent ions are located on octahedral site of lattice structure. The magnetic moments both on tetrahedral and octahedral sites are opposite to each other [41]. Inverse spinel ferrites example is $CoFe_2O_4$.

1.9.3 Mixed spinel ferrites

Mixed Spinel ferrites are also called intermediate spinel ferrites. Both trivalent and divalent cations present on A and B sites. Mixed Spinel ferrites have compositional formula $[G_\delta^{+2}H^{+3}_{1-\delta}]^A[G_{1-\delta}^{+2}H_{1+\delta}^{+3}]^BO_4$, in which G and H represent the divalent and trivalent lattice sites. In mixed spinel, structural formula 'δ' is known as degree of inversion [42]. A degree of inversion dependents on the preparation method and heat treatment procedure. For normal spinel ferrites, the degree of inversion 'δ' is zero, whereas in case of inverse spinel ferrites 'δ' it is 1. There are various examples of mixed spinel ferrites like $MgFe_2O_4$.

1.10   Cobalt ferrite ($CoFe_2O_4$)

Our main research work based upon the study of temperature dependent magnetic response of Cobalt ferrite ($CoFe_2O_4$) nanoparticles coated with zirconia. We have chosen $CoFe_2O_4$ specially for our research work due to its remarkable properties such as moderate saturation magnetization, high coercivity, excellent chemical stability and mechanical hardness [43]. $CoFe_2O_4$ shows ferrimagnetic behavior below the blocking temperature and above the blocking temperature shows superparamagnetic state. The value of saturation magnetization of $CoFe_2O_4$ is about 80emu/g for bulk. Curie temperature of cobalt ferrite is very high about $520^\circ C$. $CoFe_2O_4$ possess higher value of coercivity at bulk level.

1.10.1 Applications of cobalt ferrite

Cobalt ferrite has become attractive material for research purposes because of its remarkable applications in various fields such as memory storage, gas sensor, ferrofluids, drug delivery, cancer therapy and magnetic resonance imagining [44].

1.10.2 Crystal structure of cobalt ferrite

Cobalt ferrite has inverse cubic spinel structure. Cations present in spinel structure can occupy two different lattice sites. In the simple cubic spinel divalent ions possess tetrahedral and trivalent ions go on octahedral site of the lattice structure. In the case of cobalt ferrite which possess inverse cubic Spinel structure, divalent ion Co^{+2} and half of trivalent ions Fe^{+3} are situated in octahedral sites and other half of Fe^{+3} ions occupy tetrahedral sits. i.e. $[Fe^{+3}][Co^{+2}Fe^{+3}]O_4^{-2}$. The spin magnetic moments at both sites such as octahedral and tetrahedral are antiparallel to each other. The net magnetic moment is $3\mu_B$ [45].

1.11 Zirconia (ZrO_2) and its structure

Zirconium dioxide is a non-magnetic material also known as zirconia. Zirconia has general chemical formula ZrO_2. Melting and boiling point of zirconia are 2715°C and 4300°C respectively. It is possible to synthesize zirconia by various techniques such as sol-gel method, hydrothermal process, microwave plasma technique and auto-combustion process.

Zirconia cannot be found in pure form. After performing various refinement processes, we acquire pure zirconia. Compositional structure of zirconia depends upon temperature i.e. melting points [46]. Zirconia possess three different structural phases with different melting points such as monoclinic zirconia which has melting point up to 1170°C, tetragonal zirconia phase with melting point 1170°C to 2370°C and zirconia cubic phase having melting point from 2370°C to 2680°C. Three structures of zirconia are represented in Fig. 1.16.
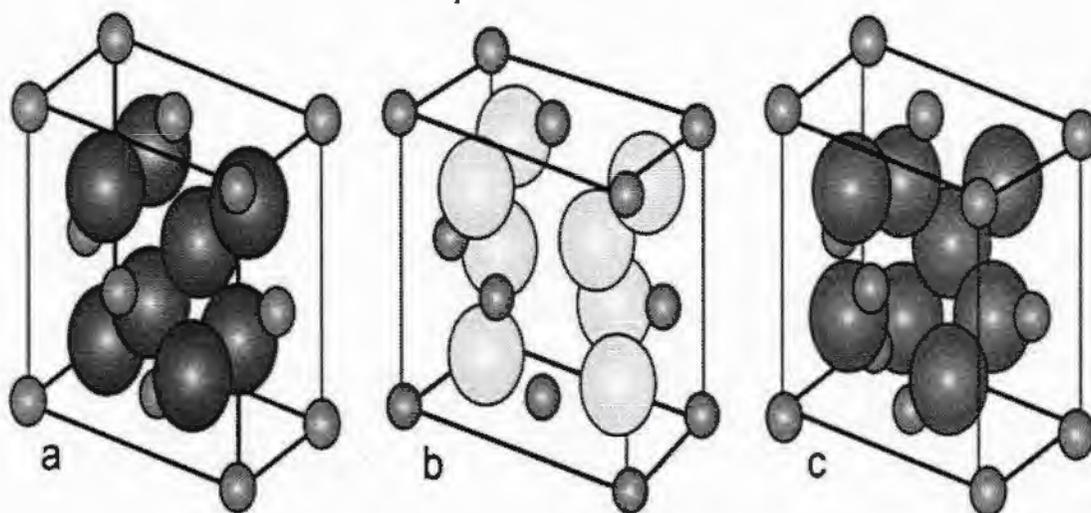
Fig. 1.16: Crystal structure of ZrO_2 (a) monoclinic (b) tetragonal (c) cubic zirconia [47].

Zirconia possess unique physical and chemical properties such as high corrosion resistance, tremendous thermal and chemical stability, great strength, good fracture toughness, high hardness and low thermal conductivity [48].

1.12   Role of zirconia coating

Uncoated $CoFe_2O_4$ nanoparticles generally agglomerated due to the strong interparticle interactions. To overcome these magnetic interactions, various coating materials can be used to avoid the interparticle interactions. We selected non-magnetic zirconia ZrO_2 coating which is used to avoid nanoparticles agglomeration and improve the chemical stability. Zirconia is most important and favorable non-magnetic material as compared with silica. The zirconia coating protects the magnetic particles from fast oxidation in surrounding atmosphere, prevents them from additional aggregation, and reduces interparticle magnetic interaction [49].

Chapter 2 ˙

Literature review

2.1   Literature review

Maaz *et al.* [50] have studied the magnetic properties of nickel ferrite nanoparticles with respect to temperature. They prepared nickel ferrite nanoparticles by using chemical co precipitation technique and studied temperature dependent of coercivity (H_c). They observed, value of H_c increased with decreased temperature. They fitted Kneller's law for nickel ferrite nanoparticles which show higher H_c value below blocking temperature (T_B). The reason is, thermal energy overcomes by anisotropy energy from (0-T_B) region. While above T_B, it shows superparamagnetic state, in which thermal fluctuation of magnetic moment increases. They also fitted Bloch's law for temperature dependent of saturation magnetization as mentioned in equation (2.1).

$$M_s(T) = M(0)[1- BT^b] \qquad (2.1)$$

Where $M_s(T)$ is temperature dependent saturation magnetization, 'B' is called bloch's constant and 'b' is the bloch's exponent. They observed the value of saturation magnetization (M_s) abruptly increased below 50 K due to contribution of surface spins into net magnetization and enhanced M_s at low temperature.

Chithra *et al.* [51] have studied the magnetic behavior of $CoFe_2O_4$ nanoparticles. They synthesized $CoFe_2O_4$ nanoparticles by using sol-gel method. They used different experimental techniques for the analysis of structural properties of material such as X-ray diffraction, Raman spectroscopy, Fourier transform infrared spectroscopy. They observed saturation magnetization (M_s) 58.36 (emu/g) at 300 K for as prepared samples. After the annealing temperature, value of M_s showed increasing trend and enhanced M_s was 80.59 (emu/g) due to less surface effects. They found two steps M-H hysteresis loop at 10 K which shows the higher values of H_c and the remanence due to canted surface spins and intergranular interactions between nanoparticles.

Nadeem *et al* .[52] examined the effect of silica matrix on magnetic and dielectric properties of cobalt ferrite nanoparticles with different concentration of silica as 10%, 30%, 50% and 60 %. They synthesized cobalt ferrite nanoparticles by using sol gel method. X-ray diffraction was used to confirm the spinel structure of nanoparticles. When the concentration of silica matrix is increased, the average crystallite size found to decrease due to development of large nucleation centers, which restrict to growth of particle. Saturation magnetization (M_s) is decreased with increasing concentration of silica matrix due to small size of nanoparticles. All magnetic and dielectric properties depend upon particle size. The concentration of silica matrix decreases magnetic and dielectric properties of cobalt ferrite nanoparticles due to finite size effect.

Zhang *et al.* [53] synthesized $CoFe_2O_4$ nanoparticles by using auto-combustion method. The properties of developed nanoparticles strongly depend upon particle size. The large size of particles possesses high blocking temperature and high anisotropy energy. In case of large particles size, there is less probability of magnetic moment to crossover the barrier and high energy is required for flipped magnetic moment. Temperature is shifted toward high value of blocking temperature. Magnetic properties of nanoparticles depend upon the annealing temperature. When annealing temperature is increased, particle size also increases and value H_c found to decrease.

Maaz *at el.* [54] synthesized cobalt ferrite nanoparticles by using wet chemical route method. They investigated the magnetic properties of sample with the variation in particle sizes. The particle size of $CoFe_2O_4$ nanoparticles lie in range of 15-48 nm. There are different parameters such as annealing time, temperature and rate of reaction used for the variations in the size of nanoparticles. It confirms, particle size is increased with increasing annealing temperature and time. Furthermore, saturation magnetization is increased with decreasing particle size and small crystallite size possesses lesser value of magnetization as compared with bulk due to surface spins disordered. They observed high value of coercivity and less value of saturation magnetization at 77 K due to growth of magnetic anisotropy at low temperature.

Zeb *et al.* [55] investigated the surface effect of SiO_2 coated and uncoated cobalt ferrite nanoparticles. They synthesized silica coated and uncoated nanoparticles by using

21

sol gel process. XRD confirms the inverse spinel structure of cobalt ferrite nanoparticles. Average crystallite sizes of silica coated nanoparticles are calculated about 25 nm which is lesser than uncoated nanoparticles. Saturation magnetization M_s trend decreased at low temperature for uncoated nanoparticles due to large surface disordered dead. They fitted Bloch's law for coated and uncoated nanoparticles. They found that temperature is decreased with increasing magnetization due to spin wave excitation. They also studied temperature (T) dependent of coercivity according to Kneller's law. Temperature is decreased with increasing coercivity H_c due to strong surface anisotropy which is contributed at low temperature. For silica coated nanoparticles the value of coercivity H_c is much greater than uncoated nanoparticles due to disordered surface spins at 4.2 K.

Xavier *et al.* [56] investigated the magnetic and structural behavior of cobalt ferrite nanoparticles by variation with sintering temperature. They prepared cobalt ferrite nanoparticles by using sol gel technique. They prepared cobalt ferrite nanoparticles by using four various sintering temperature at 300°C, 400°C, 500°C and 700°C for the 4 hours. There is different structural characterization techniques used for the sample like XRD, FT-IR, TEM, and SEM etc. The crystallite size of cobalt ferrite nanoparticles is depending upon the sintering temperature. When the sintering temperature is increased, the crystallite size of particle also increases. They investigated the magnetic properties which depend upon the sintering temperature. The saturation magnetization M_s is increased with decreasing sintering temperature due to large particle size.

Zeb *et al.* [57] have studied the surface effect of spin glass in the silica coated cobalt ferrite nanoparticles. They synthesized silica coated nanoparticles by using sol gel process. Average crystal size varies from 25 to 40 nm, which depend upon the concentration of silica matrix. Nanoparticles with larger concentration of silica matrix show two peaks in out phase ac susceptibility. First peak is blocking peak at high temperature and second peak is spin glass peak at low temperature. Both of peaks depend on the frequencies. However, the spin glass peak less shifted as compared to block peak with change in frequency due to presence of spin glass behavior. They fitted Arrhenius and dynamic scale laws for frequency dependent ac susceptibility.

$$\tau = \tau_0 \exp (E_A / K_B T_B) \tag{2.2}$$

Where E_A is the activation energy, K_B is Boltzmann constant and T_B is called blocking temperature. All magnetic measurements ensure the presence of spin glass behavior in these nanoparticles.

Toksha et al. [58] have studied the structural and magnetic properties of cobalt ferrite nanoparticles. They synthesized sample by using auto-combustion method. The particles size depends upon the annealing temperature and annealing time. They concluded that the particle size is increased with increasing annealing temperature and time. They estimated higher value of coercivity 10.2 KOe and lesser value of saturation magnetization (M_s) at 77 K due to finite size and surface effect. Large particle size has large volume so there is less probability of magnetic moment to jump over the energy barrier and blocking temperature T_B shifted to higher temperature. In conclusion, the magnetic properties are depending upon the particles size.

Nadeem et al. [59] examined the phenomena of exchange bias, memory and freezing effect of nickel ferrite nanoparticles. They synthesized nickel ferrite nanoparticles embedded in silica by using sol-gel method. Average particles size varies from 8 to12 nm. SQUID magnetometer measured the magnetic properties by applied field up to ±7 T. They investigated exchange bias effect in nickel ferrite nanoparticles due to existence of strong core-shell interaction. The nanoparticles exhibit memory effect in the ac and dc field due to the presence of spin glass behavior at low temperature. At below (50 K), the value of coercivity is suddenly increased due to contribution of large surface anisotropy in them. All these measurements show exchange bias phenomena, memory and freezing effect presence in nickel ferrite nanoparticles.

Mahboubeh et al. [60] investigated magnetic properties of cobalt ferrite nanoparticles by using three different technique like combustion method, co-precipitation and precipitation technique. They used different characterization tools such as X-ray diffraction, SEM and VSM for the analysis of structure, shape and magnetic properties respectively. Average crystallite size is calculated 69.5 nm for combustion technique, 49.5 nm for the co-precipitation method and 34.7 nm for precipitation by using XRD

CHAPTER 3

Synthesis and characterization techniques

3.1   Synthesis of ferrite nanoparticles

There is various synthesis techniques for the development of ferrite nanoparticles are mentioned in given below;

1- Sol gel.

2- Co-precipitation.

3- Hydrothermal.

4- Microwave plasma.

3.2   Synthesis of $CoFe_2O_4$ nanoparticles

We have synthesized ZrO_2 coated $CoFe_2O_4$ nanoparticles by using microwave plasma technique which explains in given below;

3.2.1 Microwave plasma technique

Microwave plasma technique is used to develop the extremely mono-dispersed nanoparticles with a very small particle size distribution. Microwave plasma technique operates at low pressure which prevents agglomeration among nanoparticles. There are following steps involved in microwave plasma synthesis. First the precursor material injected into the microwave chamber and it is evaporated by using first evaporation source. Mixture of 80 % argon and 20 % oxygen fed into the chamber. Argon gas is used as carrier gas which carries the precursor material into plasma zone. Second evaporation source is used for the coating material (ZrO_2). An electromagnetic radiation having frequency 2.45 GHz is used to generate plasma which provides energy for the formation of nanoparticles. Argon gas carries nanoparticles with it and attach on cold glass-finger.

Cold glass finger located inside the chamber is used to condense the nanoparticles and after that these nanoparticles are dried and pump out. Microwave plasma technique operates at low pressure which prevents agglomeration among nanoparticles. Fig.3.1. shows the synthesis process of ZrO_2 coated cobalt ferrite nanoparticles.

```
┌─────────────────┐      ┌──────────────┐      ┌──────────────────────┐
│ Precursor material│ ──► │ Injected into│ ◄── │ Argon gas 80 % and   │
│                 │      │   chamber    │      │ oxygen 20 %          │
└─────────────────┘      └──────────────┘      └──────────────────────┘
                                │
                                ▼
┌─────────────────┐      ┌──────────────┐      ┌──────────────────────┐
│ Argon gas carrier│ ──► │ Added into   │ ◄── │ Vapors form of       │
│ to precursor     │      │ microwave    │      │ Zirconia coating.    │
│ material         │      │ plasma chamber│     │                      │
└─────────────────┘      └──────────────┘      └──────────────────────┘
                                │
                                ▼
┌─────────────────┐      ┌──────────────┐      ┌──────────────────────┐
│ Electromagnetic │ ──► │ Nanoparticles│ ◄── │ At Pressure 80 mbar  │
│ wave 2.45 GHz   │      │ are formed in│      │                      │
│                 │      │ plasma unit  │      │                      │
└─────────────────┘      └──────────────┘      └──────────────────────┘
                                │
                                ▼
                    ┌──────────────────────┐
                    │ After coated CoFe₂O₄ │
                    │ nanoparticles are    │
                    │ dried and collected  │
                    │ from chamber         │
                    └──────────────────────┘
```
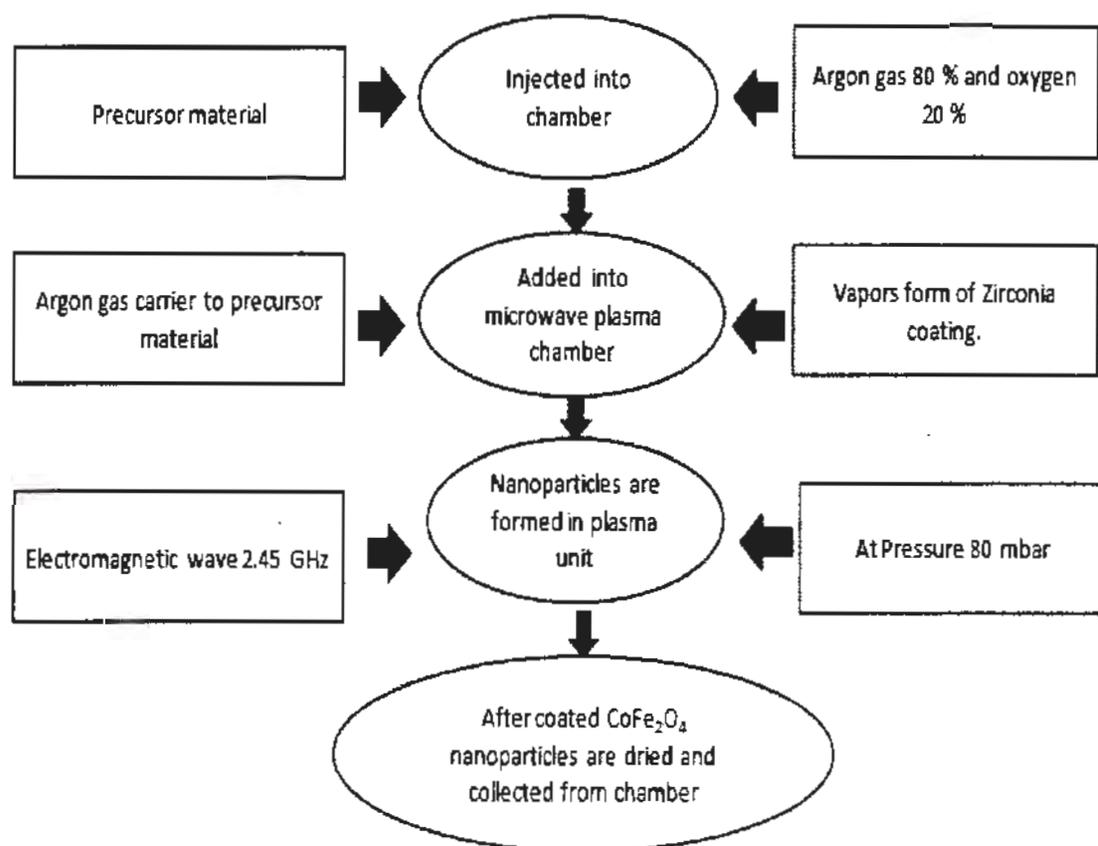
Fig. 3.1: Displays flow chart of ZrO_2 coated $CoFe_2O_4$

3.3   Characterization techniques

There are different characterization techniques used for the analysis of sample such as X-ray diffraction (XRD), Transmission Electron microscope (TEM) and superconducting quantum interference device (SQUID). XRD is used to determine the Crystal structure of sample. TEM is used to investigate the particle shape, size and composition. Magnetic measurements are measured by SQUID magnetometer.

3.4   X-rays and their production

Roentgen discovered X-ray in 1895 century; X-radiation is an electromagnetic radiation has very short range from 0.01 to 10 nm.
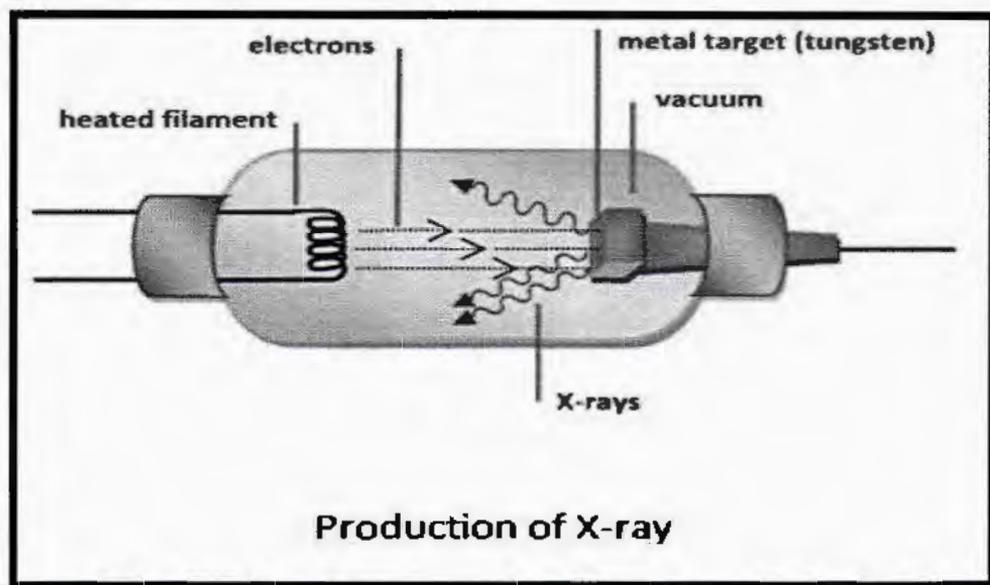
Fig. 3.2: Production of X-rays phenomena[62].

The high energy electrons are used to generate the X-ray inside the vacuum tube as shown in Fig. 3.2. High voltage is required to accelerate the electrons from one electrode side (cathode) to another (anode). When these electrons are collide with target material (tungsten) to produces X-rays [63]. There are two fundamental phenomena to produce X-rays one in Characteristics and other is Bremsstrahlung. In characteristics X-rays high accelerated electrons hit with bound electron and eject it which is due to create vacancy inside the atom. Then outermost shell of electron filled that vacancy to emit radiation in the form of X-rays known as characteristics X-rays as shown in Fig. 3.3.
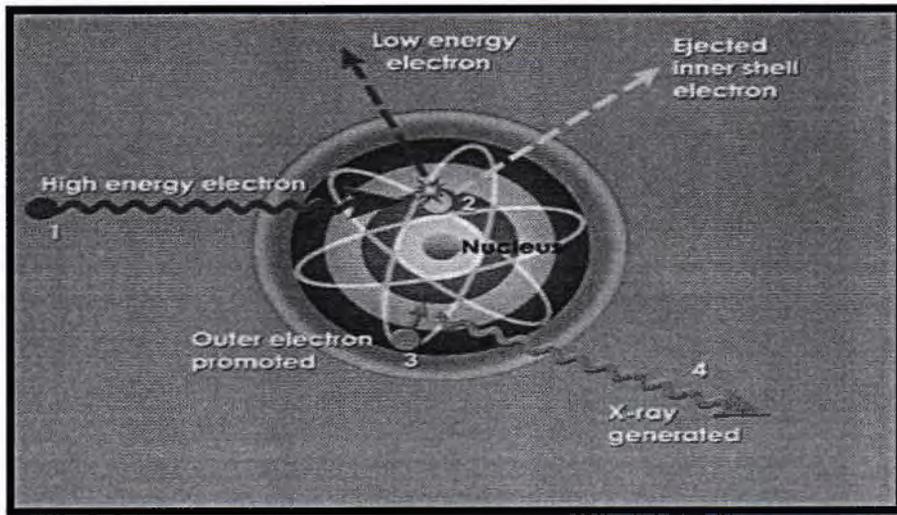
Fig. 3.3: Schematic diagram of characteristics X-rays [64].
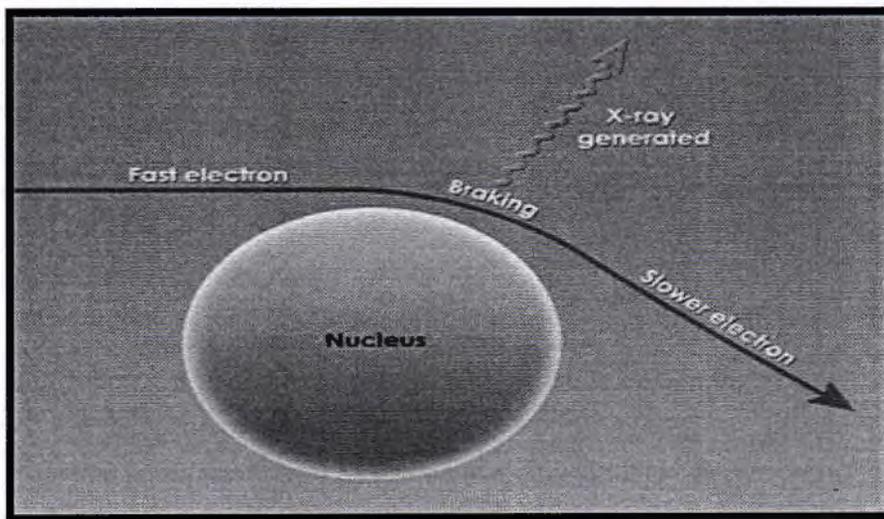
Fig. 3.4: Schematic diagram of Bremsstrahlung X-rays [64].

The bremsstrahlung process in which high energetic electrons pass near the nucleus and deflect from nuclei and dissipate energy in the form of X-rays known as Bremsstrahlung process as shown in Fig. 3.4.

3.5   X-ray diffraction (XRD)

X-ray diffraction is most important characterization process commonly used for the phase identification and crystalline structure of material. X-ray diffraction occurs in the material when magnitude of atomic inter-planer spacing matches with wavelength of incident radiation. The wavelength of X-rays about 0.1 nm mostly used for get the information about crystalline structure of material. When X-ray fall on the upper surface of crystalline material and reflected back to satisfied the constructive interference [65]. Constructive interference always occur when intensity of reflected waves are added with each other. The intensity of reflected rays depends upon three factors, wavelength of incident X-rays, incident angle and inter-planer spacing between atoms.

3.5.1 Bragg's law

The crystalline structure of sample often being examined by using X-ray diffraction which is described by Bragg's law [66]. The law states that when X-rays incident on the surface of crystal and it's angle of incidence reflect back with same angle of reflection and the constructive interference will occur then Bragg's law condition is satisfied as mentioned given below;

$$n\lambda = 2d\sin\theta \qquad (3.1)$$

Where 'n' is the integer number.

'λ' represents to the incident X-ray wavelength.

'd' is the inter-planer distance between layer of atoms.

'θ' is the angle of incident.
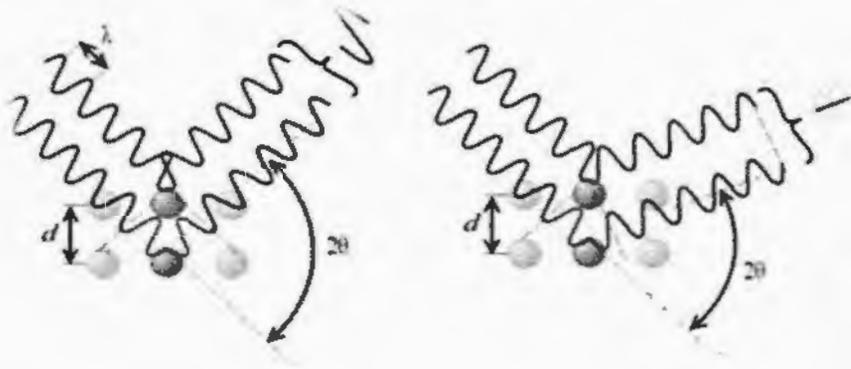
Fig. 3.5: Bragg's reflection [67].

3.6   Diffraction methods

Diffraction methods are used for the identification of crystal phase and crystal structure of material. Bragg's law condition is satisfied when angle of incidence is equal to angle of scattering wave as results maximum intensity could be carried out at constructive interference. In diffraction method there are numerous variations in experimental parameters such as wavelength 'λ' and value of 'θ'. There are different experimental process are used in diffraction method as mentioned particular below,

1- Laue method

2- Powder method

3- Rotating crystal method

3.6.1. Laue method

Laue method is used for the analysis of crystal structure of sample by using orientation of single crystal [68].
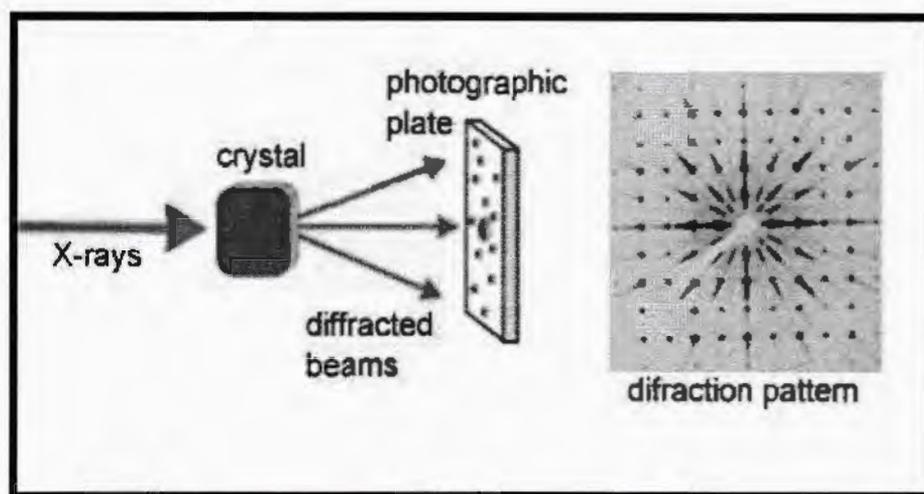
Fig. 3.6: Laue method for X-rays diffraction [69].

Consider a beam of X-rays which (0.5) nm diameter pass through the collimator. Collimator device is used for the production of different rays into parallel direction. When these X-rays interact with the single crystal to diffract in specific direction and then fall on the photographic film which records the intensity and the position of diffracted X-rays.

3.6.2   Powder method

Powder method is also known as Debye Scherrer's method. This method is used to determine the crystal structure and phase identification of crystalline sample [70].The powder method is employed to determine the lattice parameter in the accurate way. Lattice parameters possess magnitude of primitive vectors like a, b and c which defined to the unit cell of crystal.
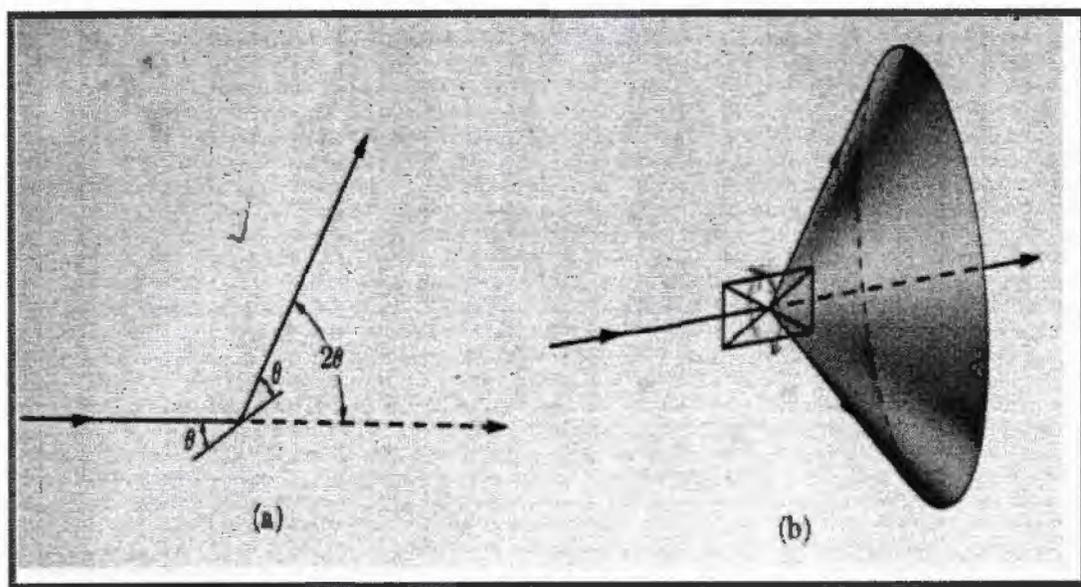
Fig. 3.7: X-ray diffraction in powder method [71].

The main procedure of powder method in considers a monochromatic beam of X-rays interacts with polycrystalline sample which means irregular arrangements of the different lattice atoms to generate a concentric cone. This is due to random orientation of the crystallite in a sample as shown in Fig. 3.7.

3.6.3 Rotating crystal method

In rotating crystal method used single crystal which mounted along the normal axis and perpendicular to the perpendicular direction of X-rays monochromatic beam. Fig.3.8. shows the cylindrical form of thin film situated around the sample and rotation of single crystal around their specific axis [72]. While process the single crystal rotates in specific set of lattice planes where the Bragg's law condition is satisfied at that point the diffraction is occurred.
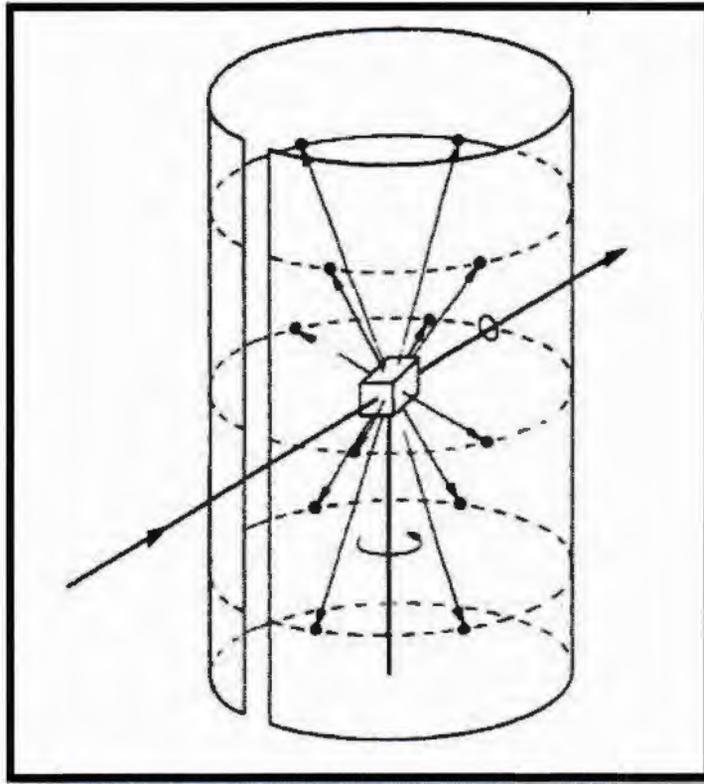
Fig. 3.8: X-ray diffraction in rotating crystal method [73].

3.7   Particle size determination

Debye Scherrer's formula is used for the calculation of average particle size of sample as mentioned in equation (3.2). The limitation of grain size can be calculated in the range between 0.1 to 0.2 μm through using formula. Debye Scherrer's formula is comparatively better as compared with Transmission electron microscopy (TEM) for the measurement of particle size up to 5%.

$$D = k\,\lambda\,/\,\beta\cos\theta_B \qquad\qquad (3.2)$$

Where 'β' is the full width half maximum, 'θ_B' represents to Bragg's angle and 'k' is the material constant.
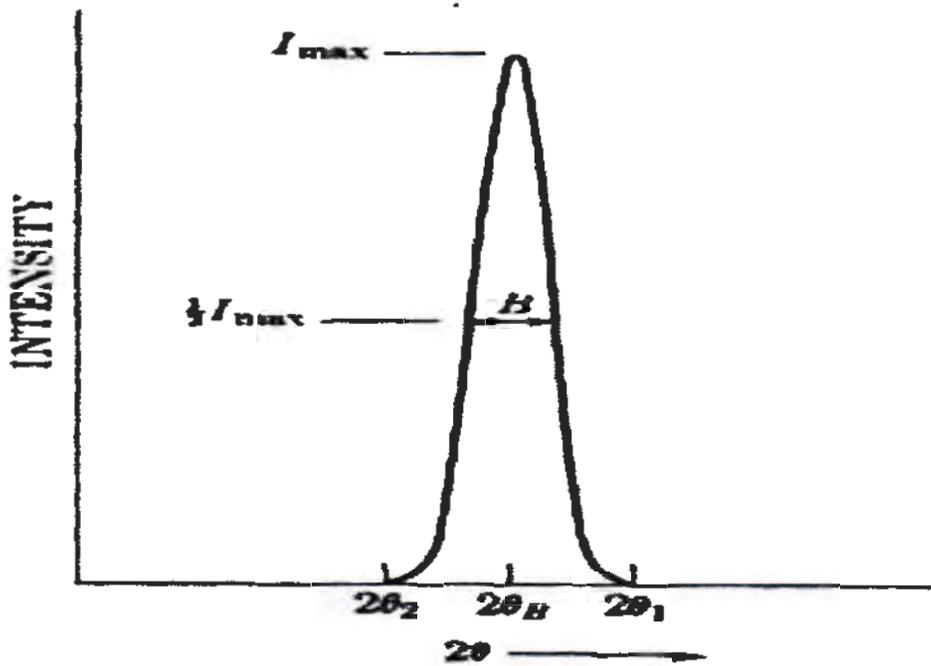
Fig.3.9: Particle size determination[74].

The value of β can be estimated by the following relation,

$$\beta = 1/2\ (2\theta_1 - 2\theta_2) \qquad\qquad (3.3)$$

3.8   Transmission electron microscopy (TEM)

Transmission Electron microscope is most important technique for the analysis of particle shape and size and composition. Consider high energy beam of electrons are generated by electron gun in the optical microscope as represented in Fig. 3.10.
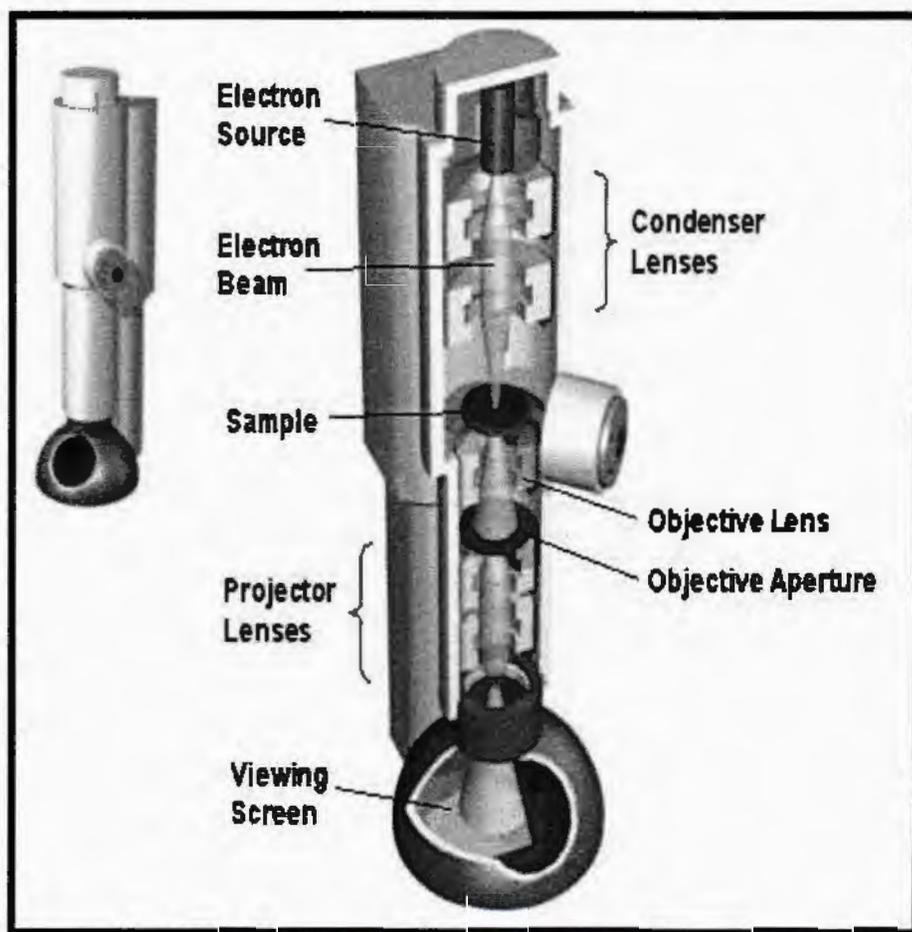
Fig. 3.10: Mechanism of TEM [75].

The electrons beam is to focus on the sample by condenser lens. The sample is situated between condenser and objective lens. These beam of electrons strike the sample and down transmitted through the objective lens. The major purpose of objective lens gathered to electrons beam that pick up at single point to produce image. The image passes down toward through the intermediate and projector lens. Where the Projector lens is used to magnify the image on phosphor screen [76]. There are various kinds of contrast exist in TEM such as mass-thickness, phase and diffraction contrast. Therefore image becomes darker, where the fewer incident electrons beam transmitted throughout the sample. Moreover the image is lighter when more electrons are transmitted through the lighter area of the sample. The most important applications of Transmission Electron Microscope is electron diffraction, that could be used to obtained three dimensional crystal structure and investigate to lattice parameter, space group and

35

orientation of crystal. If there are some defects as well as impurities in the crystalline structure, then TEM image would indicate in a contrast of reduction and exhibit amorphous behavior of the sample [77]. Furthermore dark and light images are generated as results of the phase contrast. Phase contrast is mainly the difference between diffracted phase as well as directed beam of electrons.

3.8 Superconducting Quantum interference Device (SQUID) magnetometer

SQUID magnetometer is used for evaluate the magnetic properties of various materials which depend upon the phenomena of quantum effect in the superconducting closed loop as shown in Fig. 3.11. In 1962 Brian Josephson invented the Josephson junction used in the superconducting quantum interface device (SQUID) [78]. The construction of Josephson junction is the collection of two superconductors, which are separated by the thin insulating layer an electron could pass through the tunneling barrier. The current can be generated that is depending upon the magnetic flux throughout the loop generated the current around the loop having inner diameter is 100 μm. As results loop could be measured across the potential difference [79].

SQUID is a highly sensitive device to be considered for the magnetic measurement, which consists of magnetic shield, thin film SQUID chip, two feedback coil linked with external signal to the SQUID along with regulate it, high temperature superconductor (HTS) and superconducting detection coil are required in it. SQUID magnetometer is unable to measure magnetic field to sample in the direct way. Superconducting coil is linked with SQUID through superconducting wire which is used for the movement of the sample. The current by the detection coil is inductively with SQUID by the help of superconducting coil [80]. The working principle of SQUID based upon current to voltage transducer.
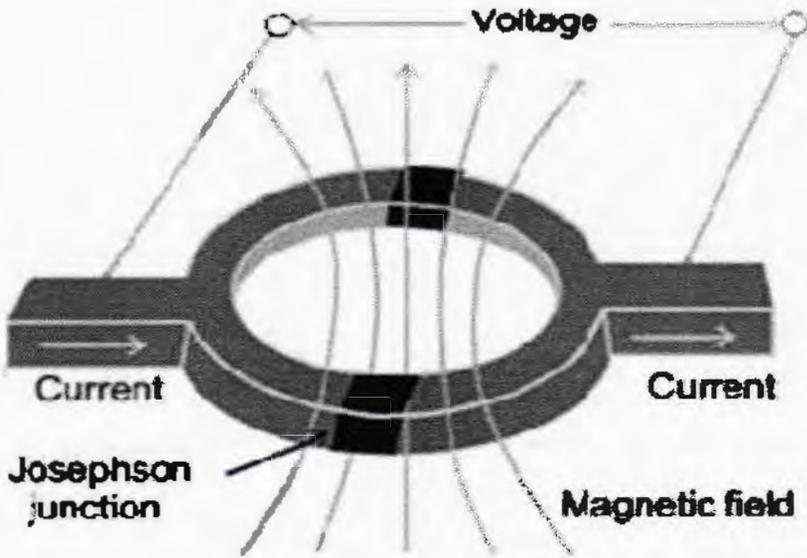
Fig. 3.11: Function of Josephson junction [81].

MPMS only takes the measurements while moving the sample through superconducting detection coil, which is placed outside from sample of chamber. A current can be developed by the magnetic moments of a sample, whenever a sample is stirred through coil which behaves as detector coils. When the magnetic flux would be changed make more chance to enhance persistent current in the detection circuit due to superconducting closed loop [82].
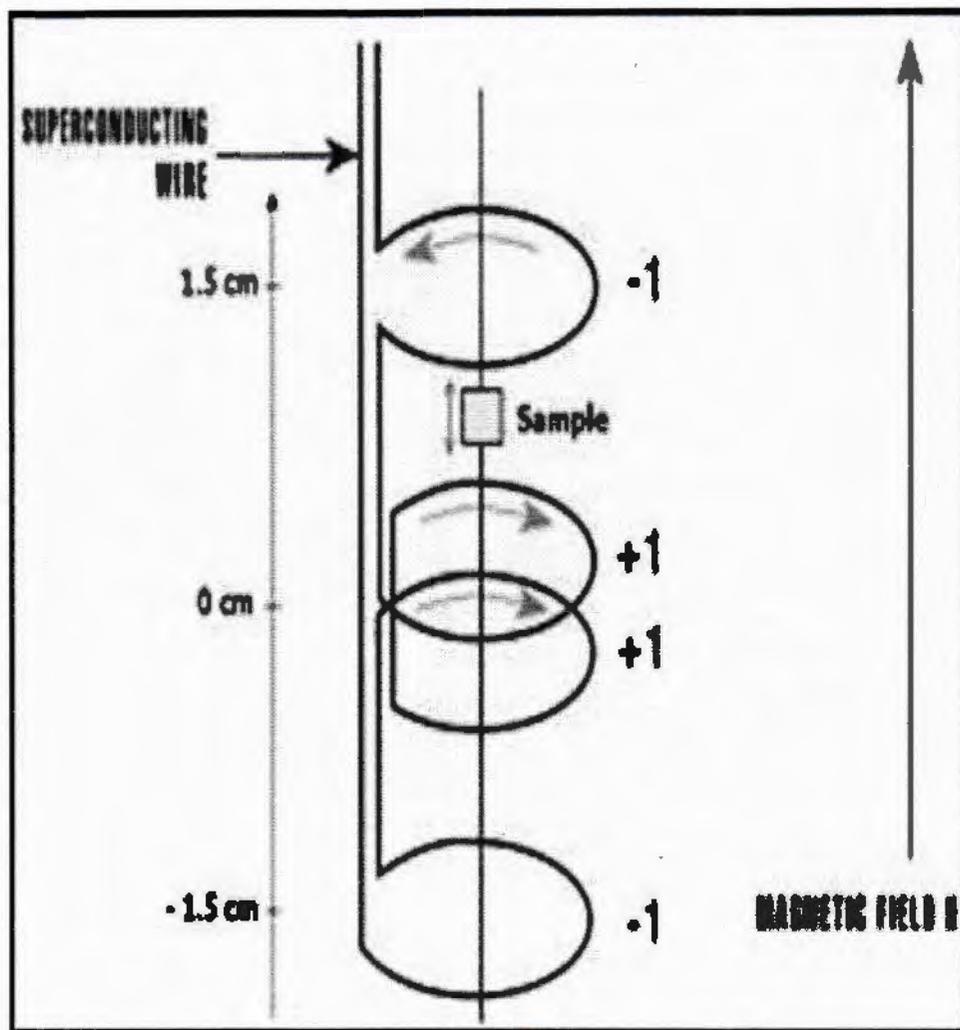
Fig. 3.12: Mechanism of superconducting detection coil in SQUID [83].

CHAPTER 4

Results and discussion

Ferrite nanoparticles have received much attention in the area of research due to their promising applications in data storage, gas sensor and magnetic resonance imaging [84]. Size and shape of nanoparticles can be controlled by various parameters such as synthesis method, surface coating, reaction time and temperature [85]. Spinel ferrites are soft and hard magnetic materials. Soft magnetic materials can be easily magnetized or demagnetized under the application of external magnetic field. While, hard ferrites hardly magnetized and demagnetized.

$CoFe_2O_4$ belongs to class of spinel ferrites and it has inverse cubic spinel structure. Structural formula for cobalt ferrite is $[Fe^{3+}]_A[Co^{2+}Fe^{3+}]_B O_4^{-2}$ where tetrahedral site 'A' occupied by half trivalent cations (Fe^{3+}) and octahedral site 'B' occupied by divalent Co^{2+} cations along with rest half of trivalent cations (Fe^{3+}). $CoFe_2O_4$ is a well-known hard magnetic material due to its remarkable properties such as excellent mechanical hardness, chemical stability, moderate saturation magnetization and high coercivity [86]. $CoFe_2O_4$ nanoparticles exhibit ferrimagnetic behavior below the blocking temperature (T_B) and above T_B, they show superparamagnetic behavior [87].

There are various methods to prepare ferrite nanoparticles. But in this research work, I have prepared ZrO_2 coated $CoFe_2O_4$ nanoparticles by using microwave plasma technique. Microwave plasma is a more convenient technique for synthesizing nanoparticles due to high degree of excitation and ionization as compared to other formal methods [88]. Non-magnetic coating of ZrO_2 is used to protect the materials from oxidation, improve ability of corrosion resistance and avoid the prepared nanoparticles from agglomeration.

X-ray diffraction technique is used to analyze the crystal structure of the cobalt ferrite nanoparticles. Transmission electron microscope (TEM) is employed to investigate the shape and size. Magnetic measurements were performed by using SQUID magnetometer [89].

39

4.1   X-ray diffraction (XRD)

X-ray diffraction (XRD) is generally used to analyzed the crystalline structure of sample [90]. The crystal structure of ZrO_2 coated $CoFe_2O_4$ nanoparticles are analyzed through XRD pattern. XRD pattern of ZrO_2 coated $CoFe_2O_4$ nanoparticle is shown in Fig. 4.1.
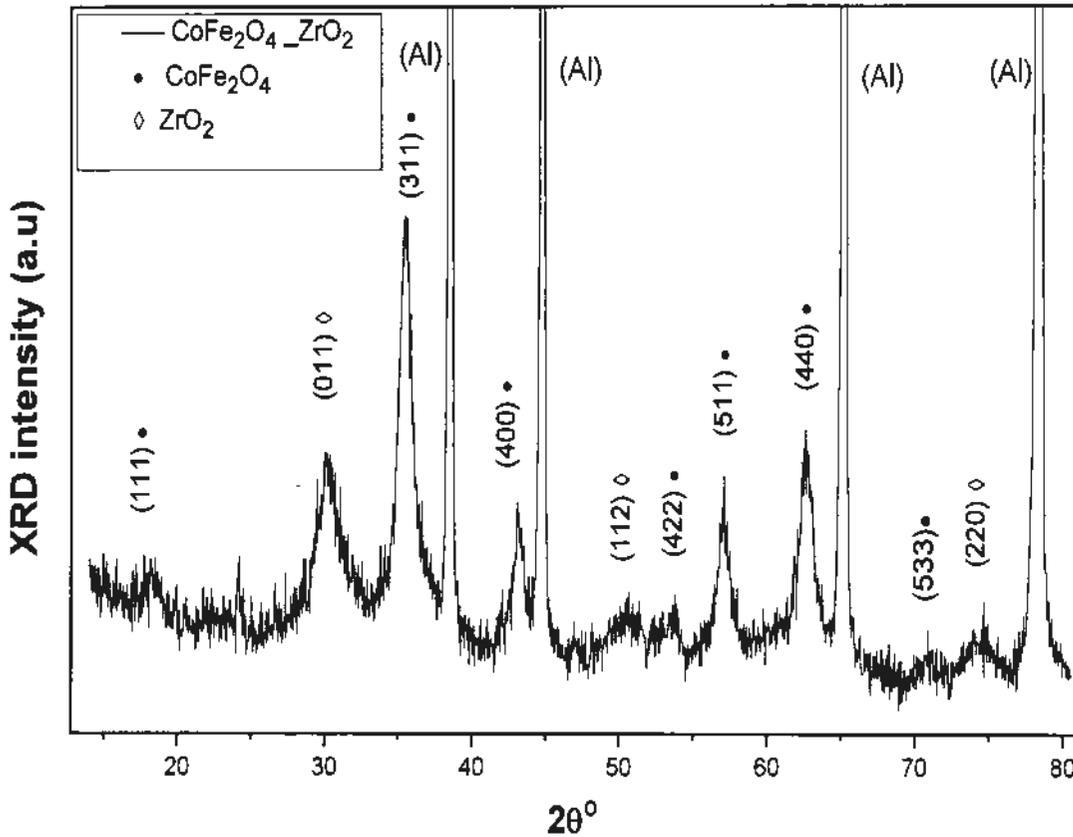
Fig. 4.1:   XRD pattern of ZrO_2 coated $CoFe_2O_4$ nanoparticles.

The indexed peaks of $CoFe_2O_4$ nanoparticles (111), (311), (400), (422), (511), (440) and (533) correspond to the diffraction angles $2\theta = 18^0$, 35.3^0, 43^0, 57^0, 62^0 and 71^0, respectively. The other indexed peaks (011), (112) and (220) at diffraction angles $2\theta = 30^0$, 50^0, 74^0 correspond to ZrO_2 coating. All peaks of $CoFe_2O_4$ confirmed inverse spinel structure with the reference (JCPDS file no.22-1086). The high intensity peaks in XRD correspond to aluminum substrate. The absence of any other peak confirmed the single phase of ZrO_2 coated $CoFe_2O_4$ nanoparticles. Average crystallite size of zirconia coated

CoFe$_2$O$_4$ nanoparticles is calculated by using D'ebye-Scherer's formula and its mathematical form is given below,

$$D = \frac{k\lambda}{\beta \cos \theta_B} \tag{4.1}$$

Where 'D' is the average crystallite size, 'k' is material's shape constant with value 0.91 for spherical symmetry, λ is the incident wavelength of X-rays, 'θ' is the diffraction angle and 'β' is the Full width at half maximum. The average crystallite size of ZrO$_2$ coated CoFe$_2$O$_4$ nanoparticles is 13 nm.

4.2   Transmission electron microscopy

Transmission electron microscopy (TEM) is used to investigate morphology and particles size/shape of nanoparticles. Fig. 4.2 shows the image of transmission electron microscopy for ZrO$_2$ coated CoFe$_2$O$_4$ nanoparticles.
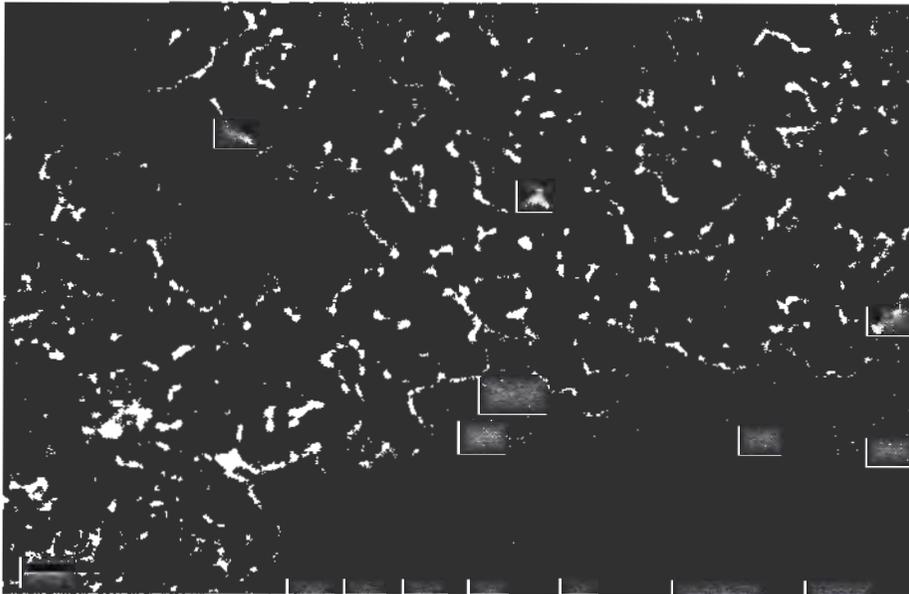
Fig. 4.2: TEM image of ZrO$_2$ coated CoFe$_2$O$_4$ nanoparticles at 50nm scale.

TEM image revealed that ZrO$_2$ coated nanoparticles are nearly spherical in shape and less agglomerated. Zirconia is non-magnetic material and it has ability to restrict the particle size and to reduce the interparticle interactions.

4.3   Magnetic properties

Magnetic measurements were performed by using superconducting quantum interference device (SQUID) magnetometer under the presence of applied magnetic field ±5 T and varying temperature [91].

4.3.1 M-H hysteresis loops

Fig. 4.2 shows the M-H loops for ZrO_2 coated $CoFe_2O_4$ nanoparticles at different temperatures 5, 25, 50, 100, 150 and 300 K with maximum applied magnetic field of ±5T.
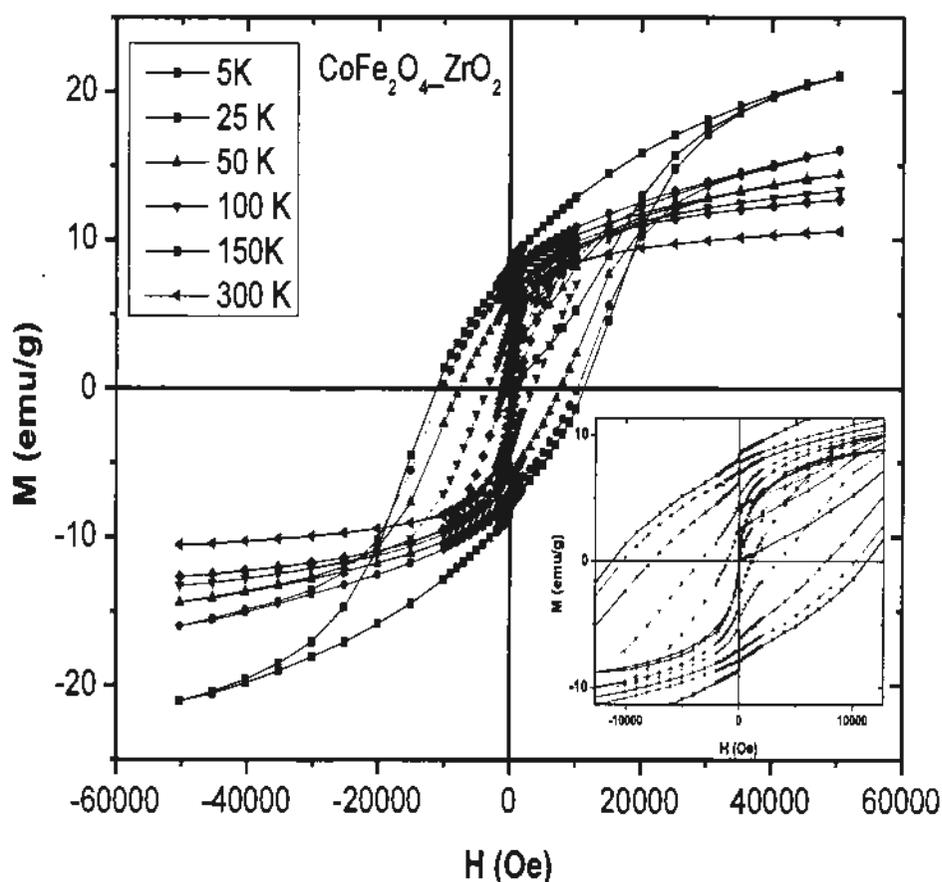
Fig. 4.3: M-H loops of ZrO_2 coated $CoFe_2O_4$ nanoparticles.

We have calculated the different values of coercivity (H_c) i.e. 11439, 10231, 7871, 3410, 1047, 38 Oe at various temperatures 5, 25, 50, 100, 150 and 300 K, respectively. It is observed that the value of H_c is increasing with decreasing temperature.

It is mainly due to large surface anisotropy and frozen surface spins which are not giving any response towards the applied magnetic field at low temperature. Saturation magnetization (M_s) values are 20, 15, 13, 12, 11 and 10 emu/g at different temperatures 5, 25, 50, 100, 150, 300 K respectively. The M-H curve shows a maximum value of M_s about 20 emu/g at 5 K due to less thermal fluctuation of magnetic moments [92]. The saturation magnetization was (20 emu/g) at 5 K which is lower than the bulk value (80 emu/g) and is attributed to enhanced surface disordered in these nanoparticles.

4.3.2 Saturation magnetization and Bloch's law fit

Fig. 4.4 shows Bloch's law fit for ZrO_2 coated $CoFe_2O_4$ nanoparticles. The saturation magnetization increases monotonically with decreasing temperature from 300 to 5 K. Temperature dependence of saturation magnetization M_s is explained by Bloch's law and its mathematical definition is given in equation 4.2 [93].

$$M_s(T) = M_s(0)(1 - BT^b) \tag{4.2}$$

Where $M_s(T)$ is the temperature dependence of spontaneous saturation magnetization, $M_s(0)$ is the value of saturation magnetization at 0 K (by extrapolating), 'B' is called Bloch's constant and 'b' is known as Bloch's exponent. B and b are used as fitting parameters [94]. We have fitted Bloch's law and best fitting parameters are B=8.04 x 10^{-2} K^{-b} and b =0.3. Bloch's exponent value is b = 0.3 which is lower than bulk value b = 1.5 which is due to no excitation of spin-waves or magnons at low temperatures. The energy band gap is larger and wavelength of magnon is greater than dimension of particle, so high threshold energy (temperature) is required for the excitation of spin-wave or magnon at nano-scale. The value of Bloch's constant 'B' is 8.04x10^{-2} K^{-b} which is greater than bulk value as 3.3x10^{-6} $K^{-3/2}$ for $CoFe_2O_4$ and is attributed to disordered surface spins are contributing to reduce the exchange interaction between magnetic moments. The Bloch's constant 'B' depends upon the particle size. When particle size is decreased it increases the value of 'B' and exchange interaction is also decreased according to formula B α 1/J. The value of M_s shows increasing trend with decreasing temperature and sharply increased below 50 K due to some extra contribution of the shell-spins moment to the net magnetization at low temperature [95].
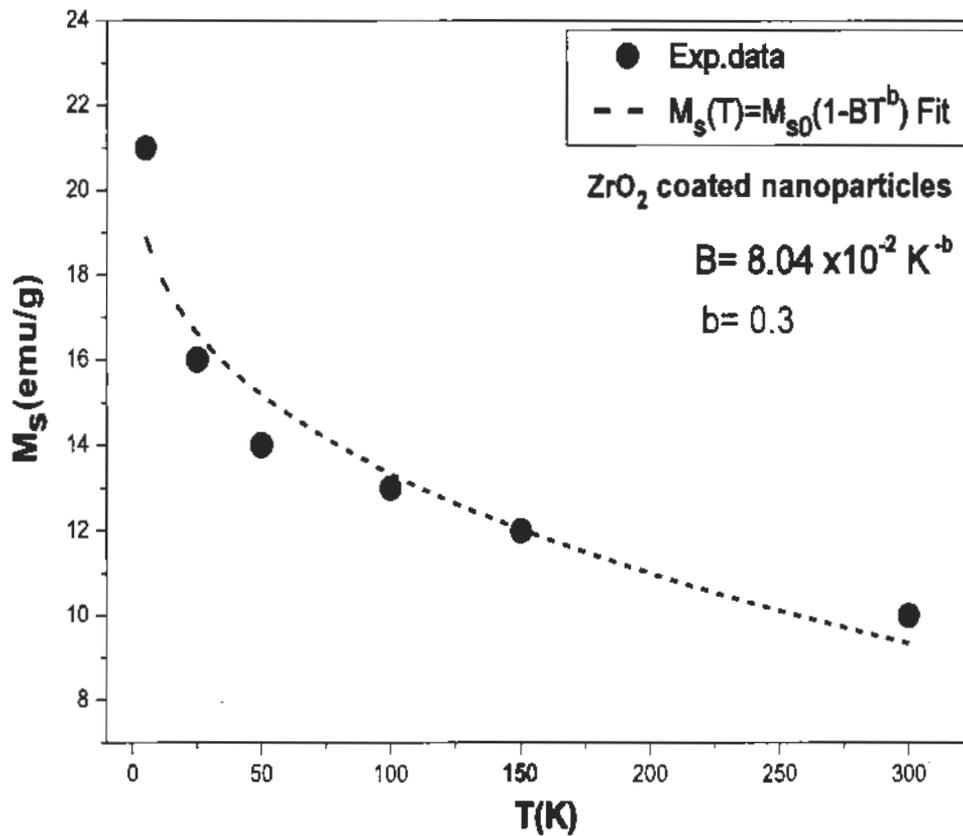
Fig. 4.4: Bloch's law fit for ZrO$_2$ coated CoFe$_2$O$_4$ nanoparticles.

4.3.3 Coercivity and Kneller's law fit

Fig. 4.5 shows variation of coercivity with temperatures i.e. 5, 25, 50, 100, 150 and 300 K for zirconia coated CoFe$_2$O$_4$ nanoparticles. Temperature dependent coercivity is studied by using Kneller's law [50].

$$H_c = H_c(0)[1 - (T/T_B)^{1/2}] \tag{4.3}$$

In equation (4.3), 'H$_c$(0)' is the value of coercivity at temperature 0 K as estimated by extrapolating the graph and 'T$_B$' is the average blocking temperature.
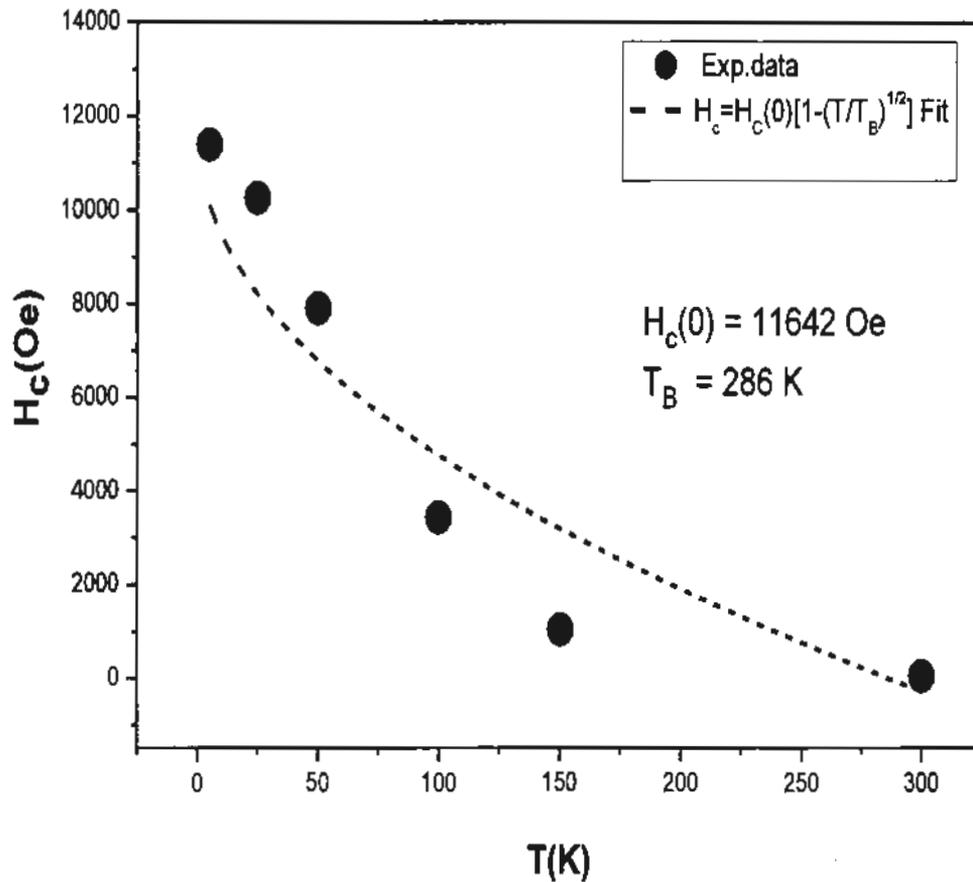
Fig. 4.5: Kneller's law fit for ZrO_2 coated $CoFe_2O_4$ nanoparticles.

We have fitted Kneller's law with the best parameters T_B= 286 K and $H_c(0)$= 11642 Oe for coated nanoparticles. In the best fit of zirconia coated $CoFe_2O_4$ nanoparticles the value of coercivity is 11642 Oe which is greater than 900 Oe of bulk $CoFe_2O_4$ due to surface effects. As temperature is decreased from 300 to 5 K, coercivity increased due to decrease in thermal fluctuations of blocked moments over the anisotropy barrier [96]. The value of coercivity increases sharply below 50 K due to strong surface anisotropy. As surface spins are frozen below 50 K due to which extra energy is needed to flip the blocked magnetic moments. As a result, we get enhanced value of coercivity (H_c) at low temperature [97].

4.3.4 Simulated and experimental ZFC magnetization

Temperature dependence of magnetization for ZrO_2 coated $CoFe_2O_4$ nanoparticles is measured by zero field cooled (ZFC) process. For ZFC measurement, first the sample is cooled from room temperature to 5 K under the absence applied field then 500 Oe field is applied and record the magnetization with increasing temperature. The temperature at which all magnetic moments are blocked and shows maximum magnetization is called blocking temperature (T_B) [98]. Below T_B, the magnetic moments are blocked as thermal energy is less than the anisotropic energy and this state is referred as block state. Above the T_B, superparamagnetic state is observed where the anisotropic energy overcome by the thermal energy and the magnetic moments fluctuate in different directions mean they do not follow the applied field. Fig. 4.6 shows ZFC curve under the presence of 500 Oe field. No blocking peak is observed in ZFC from 300 to 5 K because $CoFe_2O_4$ is hard material and in blocked state till 300K. We have compared the experimental ZFC by simulation and used Neel-brown relaxation model for uniaxial anisotropy. According to the Neel-brown model for non-interacting particles, the magnetic susceptibility of ZFC magnetization is given by,

$$\chi_{ZFC}(T) = \frac{M_s^2}{3\,K_{eff}}[\, \ln (\tau_m/\tau_o)\, \int_0^T \frac{T_B}{T} f(T_B)\, dT_B + \int_T^\infty f\,(dT_B)\, dT_B] \tag{4.4}$$

In equation 4.4 first and second terms representing to super-paramagnetic and blocked states respectively. We have done simulation of experimental data and best fitting parameters are D = 9.9 nm, M_s = 18.8 emu/g and K_{eff} = 1.6×10^7 ergs/cc. The value of M_s is 18.8 (emu/g and it is lower than the bulk value which is 80 emu/g for cobalt ferrite due to surface and finite size effects. The value of K_{eff}=1.6×10^7 erg/cc is greater than K_{Bulk}= 1.8-3.0×10^6 ergs/cc for $CoFe_2O_4$ due to presence of disordered surface spins [99].
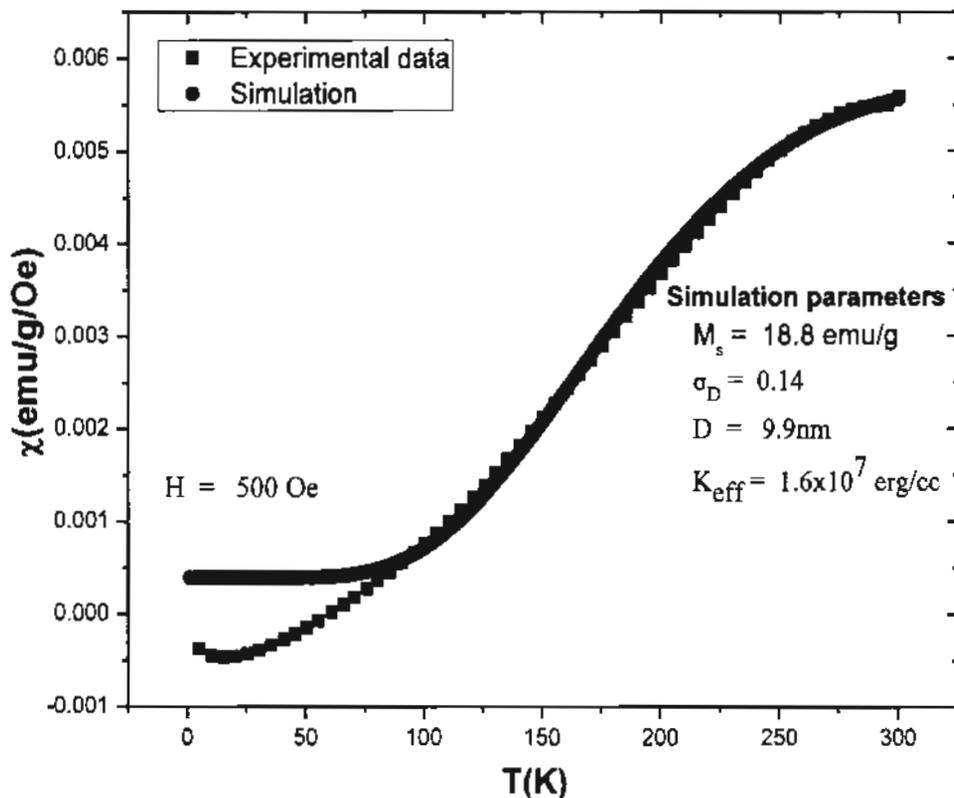
Fig. 4.6: ZFC Simulation of ZrO_2 coated $CoFe_2O_4$ nanoparticles.

4.4   Stretched exponential decay model

In stretched exponential model, the time-dependent magnetization of sample was investigated under ZFC protocol [100]. Fig. 4.6 with black color shows ZFC relaxation for ZrO_2 coated with $CoFe_2O_4$ nanoparticles. The sample is cooled from 300 K to 5 K under the absence of field (ZFC). At 5 K, 100 Oe field is applied and then magnetization is recorded as a function of time. We have fitted relaxation curved recorded at 5K by using stretched exponential decay model as given below;

$$M = M_2 - (M_1 - M_2) \exp[\ (t/\tau)^{\beta}] \tag{4.5}$$

Where 'M_1' and 'M_2' are the initial and final magnetization, 'β' is the shape parameter and 'τ' is called relaxation time. The values of shape parameter (β) lies in range of $0 < \beta < 1$ which depends upon the different disordered in the system [101]. Spin-glass systems usually exhibit shape parameter in the range from 0.2 to 0.6 at below the freezing

temperature. The best fitting parameters of stretched exponential law are $\tau = 1394$ s and β = 0.6 which signify the slow spin relaxation in our system due to existence of spin-glass behavior or disorder surface spins. Zirconia coated nanoparticles showed a slow spin relaxation in ZFC mode, which is due to presence of frozen surface spins and spin glass behavior in these nanoparticles.
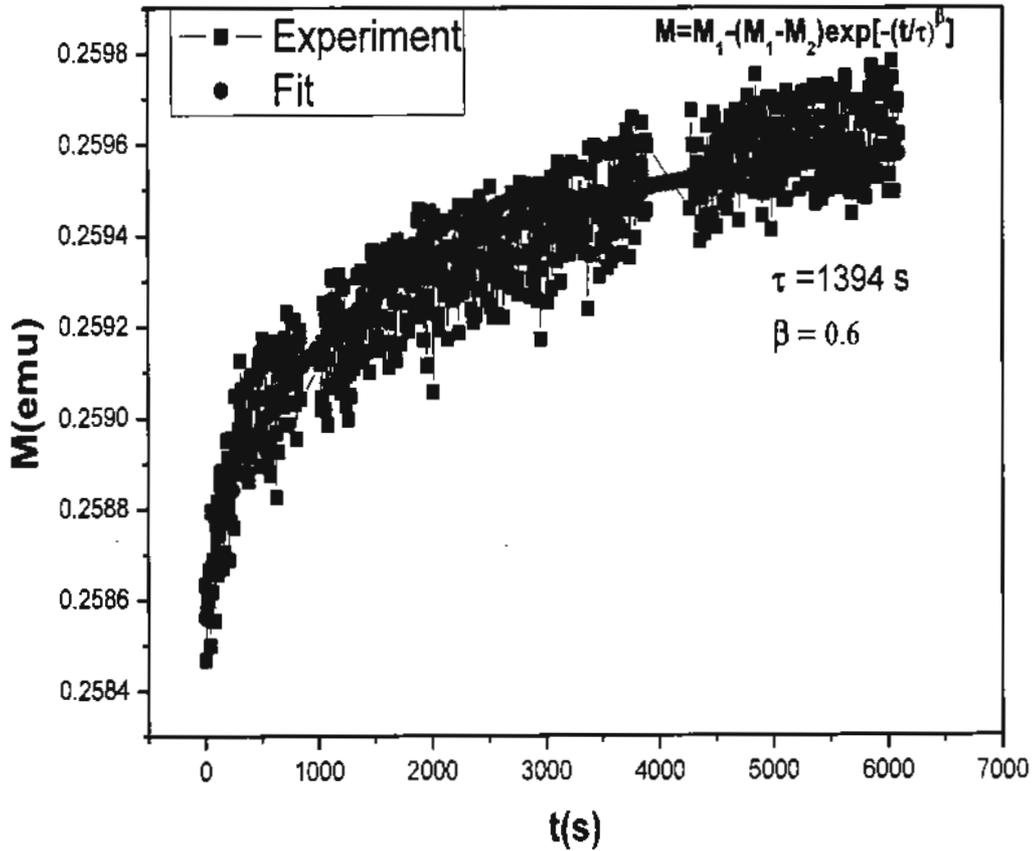
Fig. 4.7: Stretched exponential decay model for ZrO_2 coated $CoFe_2O_4$ nanoparticles.

4.5   AC-susceptibility

In AC-Susceptibility magnetic measurements, ac field is applied to the sample or material and resultant magnetic moment is measured. AC-susceptibility can be defined as

$$\chi_m = \chi' + i\chi'' \tag{4.6}$$

Where 'χ_m' is the response of the magnetic dipole moment when field is applied on the material. AC- susceptibility χ' is the in phase or real component and $i\chi''$ is the out of phase or imaginary component of ac-susceptibility [103]. For ac-susceptibility

measurements the relaxation time is not based upon the energy barrier. It depends upon the external excitation frequency. AC-susceptibility gives us information about the magnetization dynamics of the system.

To measure the frequency dependent ac-susceptibility, first the sample is to be cooled from room temperature to 5 K in the absence of applied ac field and ac-susceptibility is measured at constant frequency with varying temperature. Fig 4.8 (a) and (b) shows the in phase and out of phase AC-susceptibility at different frequencies 1 Hz, 10 Hz and 100 Hz.
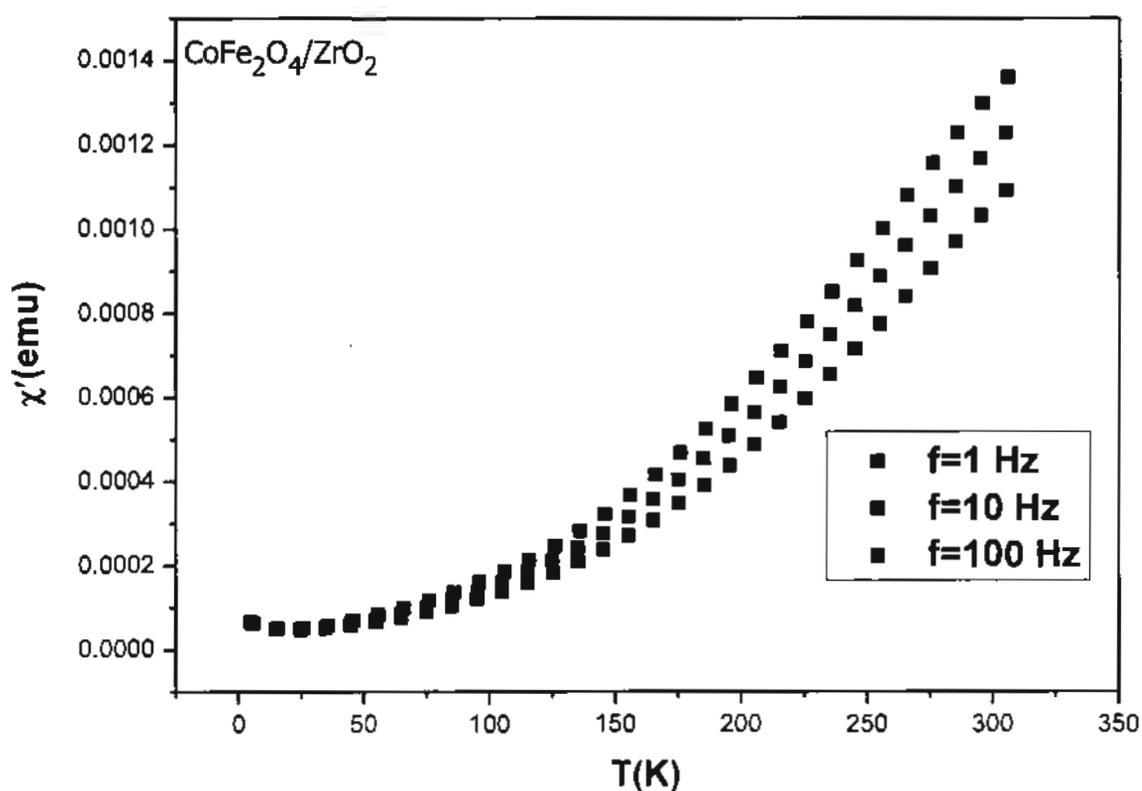
Fig. 4.8(a): In-phase frequency dependent AC-Susceptibility of ZrO_2 coated $CoFe_2O_4$.
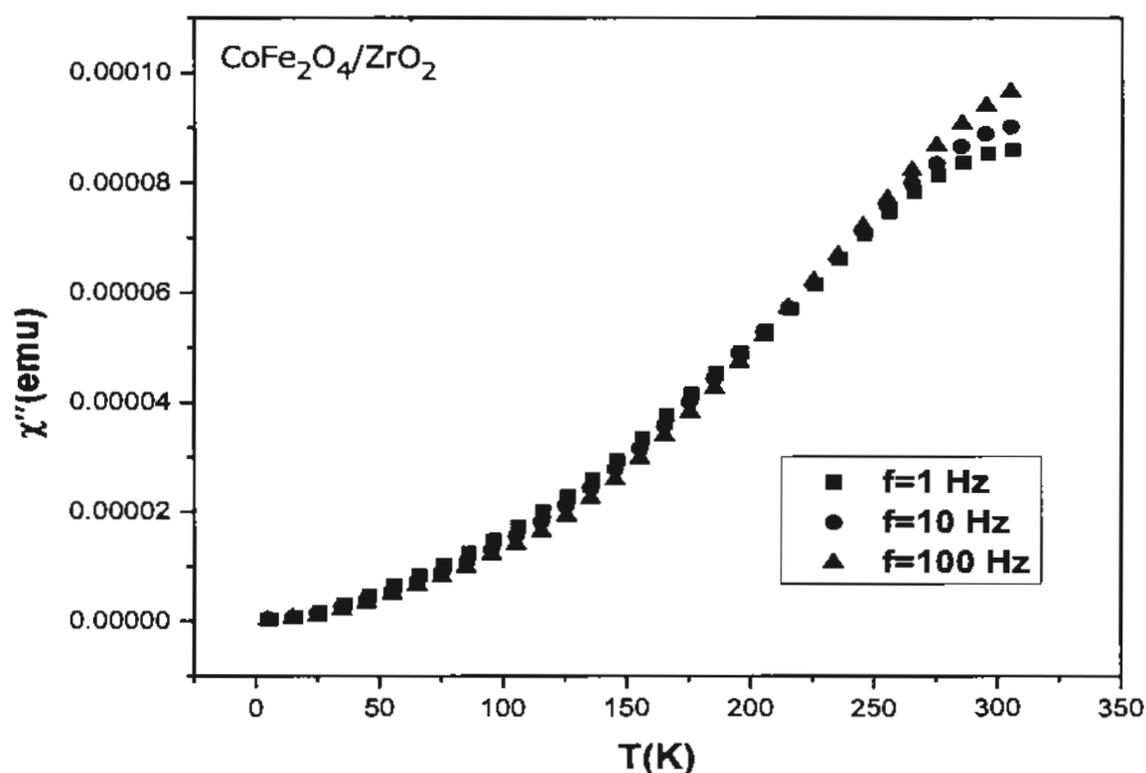
Fig. 4.8(b): Out of phase frequency dependent AC-Susceptibility of ZrO_2 coated $CoFe_2O_4$.

These both figures show that value of T_B is higher than 300K value. Fitting laws such as Arrhenius, Vogel- Fulcher and dynamic scaling law could not be fitted because in our experimental data the values of T_B on different frequencies cannot be calculated and these laws are applicable when we have values of T_B at different frequencies. However frequency dependence of the AC susceptibility shows the presence of spin-glass and/or superparamagnetic behavior.

Table 4.1: Values of fitted parameter related to the magnetic properties of ZrO_2 coated $CoFe_2O_4$ nanoparticles by using Bloch's law, Kneller's law and stretched exponential decay model fit.

Law	Parameter	Values
Bloch's law	B	$8.04 \times 10^{-2} K^{-b}$
	b	0.3
Kneller's law	T_B	268 K
	H_c	11642 Oe
Stretched exponential law	τ	1394 s
	β	0.6

4.6 Conclusions

In this research, we have studied temperature dependent magnetic properties of ZrO_2 coated $CoFe_2O_4$ nanoparticles prepared by using microwave plasma synthesis. XRD was used to analyze the structure properties of material and with average crystallite size calculated 13 nm. TEM image shows, nanoparticles are spherical in shape and less agglomerated. The M_s value of ZrO_2 coated $CoFe_2O_4$ nanoparticles is calculated 20 emu/g which is much lower than the bulk value 80 emu/g due to finite size effects. In ZFC measurement, the T_B peak is not observed till 300 K which shows the ZrO_2 coated $CoFe_2O_4$ nanoparticles are highly thermal stable close to superparamagnetic region at room temperature. The temperature dependent M_s was fitted by using Bloch's law which gives very smaller value of Bloch's exponent and large value of Bloch's constant B and is attributed to surface spins disordered and finite size effect. Kneller's law shows a best fit for zirconia coated nanoparticles. Below 50 K, the value of H_c is sharply increased due to enhanced surface anisotropy at low temperature. The nanoparticles showed a slow spin relaxation in ZFC mode, which is due to presence of frozen surface spins and spin glass behavior in these nanoparticles. The best fitting parameters of stretched exponential law were τ = 1394 s and β=0.6, which signify the slow spin relaxation in our system due to existence of spin glass behavior. We have also measured the frequency dependent ac susceptibility data which shows that the blocking temperature (T_B) peak is not present till 300 K. However, frequency dependence of AC susceptibility is observed which is due to presence of spin-glass and/or superparamagnetic behavior in these particles. In conclusion, zirconia coated nanoparticles show enhanced surface anisotropy and possible weak spin glass behavior at low temperature.

References

[1] G.A. Mansoori, Principles of nanotechnology: molecular-based study of condensed matter in small systems, World Scientific Publishing Co Inc, 2005.

[2] J. Ramsden, Essentials of nanotechnology, BookBoon, 2009.

[3] V.S. Chauhan, S.K. Chakrabarti, Use of nanotechnology for high performance cellulosic and papermaking products, Cellul. Chem. Technol. 46 (2012) 389.

[4] A.V. das Neves, Application of nanotechnology in beverage industry.

[5] C. Selin, Expectations and the Emergence of Nanotechnology, Sci. Technol. Human Values. 32 (2007) 196-220.

[6] R.P. Feynman, There's plenty of room at the bottom, Miniaturization, 282 (1961) 295-296.

[7] M. Auffan, J. Rose, J.-Y. Bottero, G.V. Lowry, J.-P. Jolivet, M.R. Wiesner, Towards a definition of inorganic nanoparticles from an environmental, health and safety perspective, Nature nanotechnology, Nat. Nanotechnol. 4 (2009) 634-641.

[8] G.A. Ozin, A.C. Arsenault, L. Cademartiri, Nanochemistry: a chemical approach to nanomaterials, Royal Society of Chemistry, 2009.

[9] T.P. Yadav, R.M. Yadav, D.P. Singh, Mechanical milling: a top down approach for the synthesis of nanomaterials and nanocomposites, J. Nanosci. Nanotechnol. 2 (2012) 22-48.

[10] H.-K. Chan, P.C.L. Kwok, Production methods for nanodrug particles using the bottom-up approach, Adv. Drug Delivery Rev. 63 (2011) 406-416.

[11] https://www.nature.com/nrn/journal/v7/n1/box/nrn1827_BX1.html.

[12] J. Stöhr, H.C. Siegmann, Magnetism, Solid State Sci. Springer, Berlin, Heidelberg, 5 (2006).

[13] http://www.sr.bham.ac.uk/xmm/fmc2.html.

[14] http://www.readorrefer.in/article/Magnetic-Materials_6823/.

[15] D.L. Leslie-Pelecky, R.D. Rieke, Magnetic properties of nanostructured materials, Chem. Mater. 8 (1996) 1770-1783.

[16] http://nptel.ac.in/courses/113104005/77.

[17] C.G. Darwin, The diamagnetism of the free electron, in: Mathematical Proceedings of the Cambridge Philosophical Society, Cambridge Univ Press. 1931, pp. 86-90.

[18] J. Pople, Molecular Orbital Theory of Diamagnetism. IV. Anisotropic Properties of Benzene, J. Chem. Phys. **41** (1964) 2559-2560.

[19] http://www.irm.umn.edu/hg2m/hg2m_b/hg2m_b.html.

[20] E.A. Boudreaux, L. Mulay, Theory and applications of molecular paramagnetism, Wiley New York, 1976.

[21] P.-W. Anderson, P. Weiss, Exchange narrowing in paramagnetic resonance, Rev. Mod. Phys. **25** (1953) 269.

[22] R.M. Bozorth, Ferromagnetism, Ferromagnetism, by Richard M. Bozorth, pp. 992. ISBN 0-7803-1032-2. Wiley-VCH, August 1993., 1 (1993).

[23] T. Moriya, Anisotropic superexchange interaction and weak ferromagnetism, Phys. Rev. **120** (1960) 91.

[24] http://elec-trical.blogspot.com/2012/06/types-of-magnetism.html.

[25] T. Kasuya, A theory of metallic ferro-and antiferromagnetism on Zener's model, Prog. Theor. Phys. **16** (1956) 45-57.

[26] https://en.wikipedia.org/wiki/Antiferromagnetism.

[27] S. Chikazumi, C.D. Graham, Physics of Ferromagnetism 2e, Oxford University Press on Demand, 2009.

[28] http://sciexplorer.blogspot.com/2011/10/magnetism-explained-4-other-kinds-of.html.

[29] S. Mørup, E. Tronc, Superparamagnetic relaxation of weakly interacting particles, Phys. Rev. Lett. **72** (1994) 3278.

[30] https://www.slideshare.net/dhanesh-ase-tut-finland/hkiceas-2012.

[31] https://www.researchgate.net/figure/49682386_fig1_Figure-1-The-qualitative-behavior-of-the-size-dependent-coercivity-of-magnetic.

[32] E. Kneller, F. Luborsky, Particle size dependence of coercivity and remanence of single-domain particles, J. Appl. Phys. **34** (1963) 656-658.

[33] http://cpb.iphy.ac.cn/article/2015/cpb_24_7_077505.html.

[34] T. Sato, T. Iijima, M. Seki, N. Inagaki, Magnetic properties of ultrafine ferrite particles, J. Magn. Magn. Mate. **65** (1987) 252-256.

[35] E.C. Snelling, Soft ferrites, (1969).

[36] M. Pardavi-Horvath, Microwave applications of soft ferrites, J. Magn. Magn. Mate. 215 (2000) 171-183.

[37] L. Jahn, H. Müller, The coercivity of hard ferrite single crystals, Phys. Status Solidi B. **35** (1969) 723-730.

[38] T.-S. Chin, Permanent magnet films for applications in microelectromechanical systems, J. Magn. Magn. Mate. **209** (2000) 75-79.

[39] P.M. Chaikin, T.C. Lubensky, Principles of condensed matter physics, Cambridge university press, 2000.

[40] R.H. Kodama, A.E. Berkowitz, Atomic-scale magnetic modeling of oxide nanoparticles, Phys. Lett. B. **59** (1999) 6321.

[41] Z. Szotek, W. Temmerman, D. Ködderitzsch, A. Svane, L. Petit, H. Winter, Electronic structures of normal and inverse spinel ferrites from first principles, Phys. Rev. B. **74** (2006) 174431.

[42] C. Chinnasamy, A. Narayanasamy, N. Ponpandian, K. Chattopadhyay, K. Shinoda, B. Jeyadevan, K. Tohji, K. Nakatsuka, T. Furubayashi, I. Nakatani, Mixed spinel structure in nanocrystalline $NiFe_2O_4$, Physical Review B, Phys. Rev. B. (2001) 184108.

[43] A. Grunwald, A.-G. Olabi, Design of a magnetostrictive (MS) actuator, Sensors and Actuators A: Physical, **144** (2008) 161-175.

[44] Z. Chen, L. Gao, Synthesis and magnetic properties of $CoFe_2O_4$ nanoparticles by using PEG as surfactant additive, Mater. Sci. Eng., B. **141** (2007) 82-86.

[45] R. Mohamed, M. Rashad, F. Haraz, W. Sigmund, Structure and magnetic properties of nanocrystalline cobalt ferrite powders synthesized using organic acid precursor method, J. Magn. Magn. Mater. **322** (2010) 2058-2064.

[46] S. Shukla, S. Seal, R. Vij, S. Bandyopadhyay, Reduced activation energy for grain growth in nanocrystalline yttria-stabilized zirconia, Nano letters, **3** (2003) 397-401.

[47] https://www.intechopen.com/books/advances-in-ceramics-electric-and-magnetic-ceramics-bioceramics-ceramics-and-environment/application-of-zirconia-in-dentistry-biological-mechanical-and-optical-considerations.

[48] B. Cullity, Introduction to Magnetic Materials, Addison-Wesley, Reading, MA, 1972, D. Shectman, V. Van Hardeenand D. Jossel, Muter. Lett, **20** (1994) 329.

[49] G.S. Chaubey, J.-K. Kim, Structure and Magnetic Characterization of Core-Shell Fe@ ZrO_2 Nanoparticles Synthesized by Sol-Gel Process, Bull. Korean Chem. Soc. **28** (2007) 2279-2282.

[50] K. Maaz, A. Mumtaz, S. Hasanain, M. Bertino, Temperature dependent coercivity and magnetization of nickel ferrite nanoparticles, J. Magn. Magn. Mater. **322** (2010) 2199-2202.

[51] M. Chithra, C. Anumol, B. Sahu, S.C. Sahoo, Exchange spring like magnetic behavior in cobalt ferrite nanoparticles, J. Magn. Magn. Mater. **401** (2016) 1-8.

[52] K. Nadeem, F. Zeb, M.A. Abid, M. Mumtaz, M.A. ur Rehman, Effect of amorphous silica matrix on structural, magnetic, and dielectric properties of cobalt ferrite/silica nanocomposites, J. Non-Cryst. Solids. **400** (2014) 45-50.

[53] K. Zhang, T. Holloway, A. Pradhan, Magnetic behavior of nanocrystalline $CoFe_2O_4$, J. Magn. Magn. Mater. **323** (2011) 1616-1622.

[54] K. Maaz, A. Mumtaz, S. Hasanain, A. Ceylan, Synthesis and magnetic properties of cobalt ferrite ($CoFe_2O_4$) nanoparticles prepared by wet chemical route, J. Magn. Magn. Mater. **308** (2007) 289-295.

[55] F. Zeb, A. Qureshi, K. Nadeem, M. Mumtaz, H. Krenn, Surface effects in uncoated and amorphous SiO_2 coated cobalt ferrite nanoparticles, J. Non-Cryst. Solids. **435** (2016) 69-75.

[56] S. Xavier, S. Thankachan, B.P. Jacob, E. Mohammed, Effect of sintering temperature on the structural and magnetic properties of cobalt ferrite nanoparticles, Наносистемы: физика, химия, математика, 4 (2013).

[57] F. Zeb, W. Sarwer, K. Nadeem, M. Kamran, M. Mumtaz, H. Krenn, I. Letofsky-Papst, Surface spin-glass in cobalt ferrite nanoparticles dispersed in silica matrix, J. Magn. Magn. Mater. **407** (2016) 241-246.

[58] B. Toksha, S.E. Shirsath, S. Patange, K. Jadhav, Structural investigations and magnetic properties of cobalt ferrite nanoparticles prepared by sol–gel auto combustion method, Solid State Commun. 147 (2008) 479-483.

[59] K. Nadeem, H. Krenn, Exchange bias, memory and freezing effects in $NiFe_2O_4$ nanoparticles, J. Supercond. **24** (2011) 717-720.

[60] M. Houshiar, F. Zebhi, Z.J. Razi, A. Alidoust, Z. Askari, Synthesis of cobalt ferrite ($CoFe_2O_4$) nanoparticles using combustion, coprecipitation, and precipitation methods: a comparison study of size, structural, and magnetic properties, J. Magn. Magn. Mater. **371** (2014) 43-48.

[61] Y. Zhang, Y. Liu, C. Fei, Z. Yang, Z. Lu, R. Xiong, D. Yin, J. Shi, The temperature dependence of magnetic properties for cobalt ferrite nanoparticles by the hydrothermal method, J. Appl. Phys. **108** (2010) 084312.

[62] http://www.arpansa.gov.au/RadiationProtection/Basics/xrays.cfm.

[63] H.P. Klug, L.E. Alexander, X-ray diffraction procedures, (1954).

[64] http://www.radiologymasterclass.co.uk/tutorials/physics/x-ray_physics_production.

[65] B.D. Cullity, J.W. Weymouth, Elements of X-ray Diffraction, Am. J. Phys. **25** (1957) 394-395.

[66] F. Rustichelli, On the deviation from the Bragg law and the widths of diffraction patterns in perfect crystals, Philosophical Magazine, **31** (1975) 1-12.

[67] https://en.wikipedia.org/wiki/Bragg%27s_law.

[68] J.L. Amorós, The Laue Method, Elsevier, 2012.

[69] http://www.xtal.iqfr.csic.es/Cristalografia/parte_02-en.html.

[70] Z. Kaszkur, Powder diffraction beyond the Bragg law: study of palladium nanocrystals, J. Appl. Crystallogr. **33** (2000) 1262-1270.

[71] http://pd.chem.ucl.ac.uk/pdnn/diff2/kinemat2.htm.

[72] A. Bradley, The absorption factor for the powder and rotating-crystal methods of X-ray crystal analysis, Proc. Phys. Soc. **47** (1935) 879.

[73] http://oldwww.iucr.org/iucr-top/comm/cteach/pamphlets/2/node10.html.

[74] http://www.slideserve.com/tyler/x-ray-diffraction-xrd.

[75] http://barrett-group.mcgill.ca/tutorials/nanotechnology/nano02.htm.

[76] D.B. Williams, C.B. Carter, The transmission electron microscope, in: Transmission electron microscopy, Springer, 1996, pp. 3-17.

[77] Z. Wang, Transmission electron microscopy of shape-controlled nanocrystals and their assemblies, in, Citeseer, 2000.

[78] K. Enpuku, T. Minotani, T. Gima, Y. Kuroki, Y. Itoh, M. Yamashita, Y. Katakura, S. Kuhara, Detection of magnetic nanoparticles with superconducting quantum interference device (SQUID) magnetometer and application to immunoassays, Jpn. J. **38** (1999) L1102.

[79] J. Knuutila, S. Ahlfors, A. Ahonen, J. Hällström, M. Kajola, O.V. Lounasmaa, V. Vilkman, C. Tesche, Large-area low-noise seven-channel dc SQUID magnetometer for brain research, Rev. Sci. Instrum. **58** (1987) 2145-2156.

[80] R. Ilmoniemi, R. Hari, K. Reinikainen, A four-channel SQUID magnetometer for brain research, Electroencephalography and clinical neurophysiology, Rev. Sci. Instrum. **58** (1984) 467-473.

[81] http://inspirehep.net/record/865175.

[82] D. Cohen, E.A. Edelsack, J.E. Zimmerman, Magnetocardiograms taken inside a shielded room with a superconducting point-contact magnetometer, Appl. Phys. Lett. **16** (1970) 278-280.

[83] https://www.wmi.badw.de/methods/squid.htm.

[84] Y. Chen, J. Snyder, C. Schwichtenberg, K. Dennis, R. McCallum, D. Jiles, Metal-bonded Co-ferrite composites for magnetostrictive torque sensor applications, IEEE Transactions on Magnetics, 35 (1999) 3652-3654.

[85] S.W. Lee, S. Bae, Y. Takemura, I.-B. Shim, T.M. Kim, J. Kim, H.J. Lee, S. Zurn, C.S. Kim, Self-heating characteristics of cobalt ferrite nanoparticles for hyperthermia application, J. Magn. Magn. Mater. **310** (2007) 2868-2870.

[86] L. Zhao, H. Zhang, Y. Xing, S. Song, S. Yu, W. Shi, X. Guo, J. Yang, Y. Lei, F. Cao, Studies on the magnetism of cobalt ferrite nanocrystals synthesized by hydrothermal method, J. Solid State Chem. **181** (2008) 245-252.

[87] J.B. Silva, W. De Brito, N.D. Mohallem, Influence of heat treatment on cobalt ferrite ceramic powders, Mater. Sci. Eng., B. **112** (2004) 182-187.

[88] M. Wu, Y. Zhang, S. Hui, T. Xiao, S. Ge, W. Hines, J. Budnick, M. Yacaman, Magnetic properties of SiO_2-coated Fe nanoparticles, J. Appl. Phys. **92** (2002) 6809-6812.

[89] G. Bernardini, D. Borrini, A. Caneschi, F. Di Benedetto, D. Gatteschi, S. Ristori, M. Romanelli, EPR and SQUID magnetometry study of Cu_2FeSnS_4 (stannite) and Cu_2ZnSnS_4 (kesterite), Phys. Chem. Miner. **27** (2000) 453-461.

[90] P. Kumar, S. Sharma, M. Knobel, M. Singh, Effect of La^{3+} doping on the electric, dielectric and magnetic properties of cobalt ferrite processed by co-precipitation technique, J. Alloys Compd. **508** (2010) 115-118.

[91] R. Kodama, Magnetic nanoparticles, J. Magn. Magn. Mater. **200** (1999) 359-372.

[92] E. Fulcomer, S. Charap, Thermal fluctuation aftereffect model for some systems with ferromagnetic-antiferromagnetic coupling, J. Appl. Phys. **43** (1972) 4190-4199.

[93] D.T.T. Nguyet, N.P. Duong, L.T. Hung, T.D. Hien, T. Satoh, Crystallization and magnetic behavior of nanosized nickel ferrite prepared by citrate precursor method, J. Alloys Compd. **509** (2011) 6621-6625.

[94] J. Chen, C. Sorensen, K. Klabunde, G. Hadjipanayis, E. Devlin, A. Kostikas, Size-dependent magnetic properties of $MnFe_2O_4$ fine particles synthesized by coprecipitation, Phys. Rev. B. **54** (1996) 9288.

[95] E. Della Torre, L. Bennett, R. Watson, Extension of the Bloch $T^{3/2}$ law to magnetic nanostructures: Bose-Einstein condensation, Phys. Rev. Lett. **94** (2005) 147210.

[96] X. Batlle, M. Garcia del Muro, J. Tejada, H. Pfeiffer, P. Görnert, E. Sinn, Magnetic study of M-type doped barium ferrite nanocrystalline powders, J. Appl. Phys. **74** (1993) 3333-3340.

[97] X. Batlle, M.G. del Muro, J. Tejada, H. Pfeiffer, P. Gornert, E. Sinn, Static magnetic properties of nanocrystalline Co-Ti doped barium ferrite BaFe/sub 12-2x/Co/subx/Ti/sub x/O/sub 19/(x= 0.8), IEEE Trans. Magn. **30** (1994) 708-710.

[98] D. Kim, Y. Zhang, W. Voit, K. Rao, M. Muhammed, Synthesis and characterization of surfactant-coated superparamagnetic monodispersed iron oxide nanoparticles, J. Magn. Magn. Mater. **225** (2001) 30-36.

[99] N.T. Lan, N.P. Duong, T.D. Hien, Influences of cobalt substitution and size effects on magnetic properties of coprecipitated Co–Fe ferrite nanoparticles, J. Alloys Compd. **509** (2011) 5919-5925.

[100] M. Perovic, A. Mrakovic, V. Kusigerski, J. Blanusa, V. Spasojevic, Relaxation phenomena in super spin glass nanoparticle manganite $La_{0.7}Ca_{0.3}MnO_3$, Mater. Chem. Phys. **136** (2012) 196-204.

[101] A. Bhattacharyya, S. Giri, S. Majumdar, Spin-glass-like state in GdCu: Role of phase separation and magnetic frustration, Phys. Rev. B. **83** (2011) 134427.

[102] S. Sheng, Z. Ouyang, J. Chen, M. Ruan, X. Shi, Z. Xia, Magnetic anisotropy and spin-glass behavior in spin-chain compound Ca 3 Co 1.62 Mn 0.38 O 6, Journal of Alloys and Compounds, **556** (2013) 287-291.

[103] E. Lähderanta, L. Vlasenko, R. Laiho, Temperature dependence, with implication of vortex glass behaviour, of remanent magnetization in Y-Ba-Cu-O powders and ceramics, Physica C. **199** (1992) 262-268.